Published in final edited form as:

Immunity. 2020 June 16; 52(6): 1022–1038.e7. doi:10.1016/j.immuni.2020.04.015.

Plasmacytoid dendritic cells and type I interferon promote extrafollicular B cell responses to extracellular self-DNA

Chetna Soni[1], **Oriana A. Perez**[1], **William N. Voss**[2], **Joseph N. Pucella**[1], **Lee Serpas**[1], **Justin Mehl**[1], **Krystal L. Ching**[1], **Jule Goike**[3], **George Georgiou**[2,3], **Gregory C. Ippolito**[2,4], **Vanja Sisirak**[5,7], **Boris Reizis**[1,6,7,8]

[1]Dept. of Pathology, New York University School of Medicine, New York, NY 10016, USA

[2]Department of Molecular Biosciences, University of Texas at Austin, Austin, TX 78712, USA

[3]Department of Chemical Engineering, University of Texas at Austin, Austin, TX 78712, USA

[4]Department of Oncology, Dell Medical School, University of Texas at Austin, Austin, TX 78712, USA

[5]CNRS-UMR 5164, ImmunoConcEpt, Université de Bordeaux, 33076 Bordeaux, France

[6]Dept. of Medicine, New York University School of Medicine, New York, NY 10016, USA

Summary

Class-switched antibodies to double-stranded DNA (dsDNA) are prevalent and pathogenic in systemic lupus erythematosus (SLE), yet mechanisms of their development remain poorly understood. Humans and mice lacking secreted DNase DNASE1L3 develop rapid anti-dsDNA antibody responses and SLE-like disease. We report that anti-DNA responses in *Dnase1l3*$^{-/-}$ mice required CD40L-mediated T cell help but proceeded independently of germinal center formation via short-lived antibody-forming cells (AFCs) localized to extrafollicular regions. Type I interferon (IFN-I) signaling and IFN-I-producing plasmacytoid dendritic cells (pDCs) facilitated the differentiation of DNA-reactive AFCs in vivo and in vitro and were required for downstream manifestations of autoimmunity. Moreover, the endosomal DNA sensor TLR9 promoted anti-dsDNA responses and SLE-like disease in *Dnase1l3*$^{-/-}$ mice redundantly with another nucleic acid-sensing receptor, TLR7. These results establish extrafollicular B cell differentiation into short-lived AFCs as a key mechanism of anti-DNA autoreactivity, and reveal a major contribution of pDCs, endosomal TLRs and IFN-I to this pathway.

[7]Corresponding authors: V.S. (vsisirak@immuconcept.org), B.R. (boris.reizis@nyulangone.org).

Author contributions

V.S. initiated, performed and analyzed experiments. C.S., O.A.P., L.S., J.N.P., K.C., J.M., W.N.V., J.G. performed and analyzed experiments. G.G. and G.C.I. supervised the analysis of B cell repertoire. B.R. analyzed the results and supervised the project. C.S. and B.R. wrote the manuscript with input from all coauthors.

[8]Lead contact

Declaration of Interests

The authors declare no competing financial interest.

Graphical Abstract

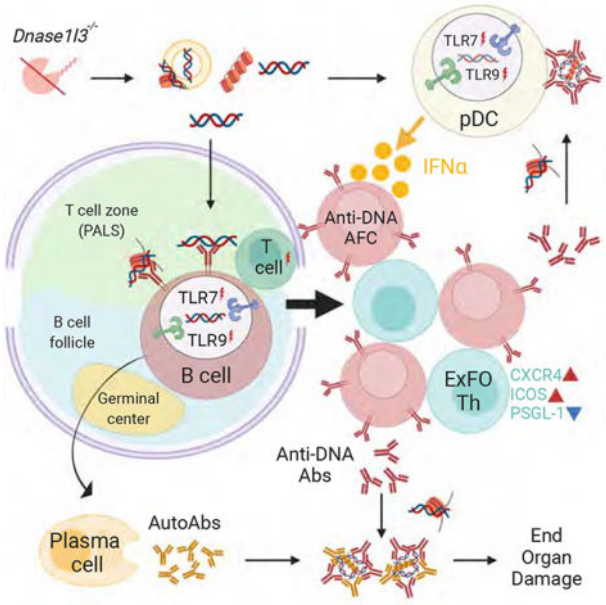

eTOC blurb

Autoantibodies to self-DNA are a defining feature of systemic lupus erythematosus (SLE), yet the mechanisms of their development remain poorly understood. Soni et al. show that anti-DNA autoreactivity is driven by extrafollicular B cell differentiation into short-lived plasmablasts, which is facilitated by plasmacytoid dendritic cells, type I interferon and endosomal Toll-like receptors 7 and 9.

Introduction

Systemic lupus erythematosus (SLE) is a systemic autoimmune disease defined by class-switched antibodies (Abs) to nuclear antigens. More than half of SLE patients develop high titers of IgG to double-stranded DNA (dsDNA), which correlate with disease activity, severity and lupus nephritis (Pisetsky, 2016; Yung and Chan, 2015). B cells that produce these Abs represent major targets of emerging therapies in SLE (Hale et al., 2018). Autoreactive B cell responses can be driven by the germinal center (GC) reaction (Vinuesa et al., 2009), which is supported by $CD4^+$ follicular helper T cells (GC-Tfh) (Lesley et al., 2006; Seo et al., 2002; Vinuesa et al., 2016). Apart from the GC, autoreactive B cell differentiation can occur in the extrafollicular (ExFO) regions (Jenks et al., 2019; Jenks et al., 2018; William et al., 2002). The ExFO pathway in a lymphoproliferation-driven SLE model MRL.*lpr* is promoted by extrafollicularly localized $CD4^+$ T-helper cells (ExFO-Th) expressing CXCR4, CD40L and ICOS (Odegard et al., 2008). An ExFO T cell population in patients with lupus nephritis has been recently defined (Caielli et al., 2019). However, the relative contribution of the ExFO pathway and its dedicated helper T cells to the initiation and propagation of anti-dsDNA responses remains to be explored.

High concentration of circulating type I interferons (IFN-I) and the expression of IFN-stimulated gene signature in SLE patients correlate with high anti-DNA Ab titers and disease severity (Bennett et al., 2003; Kirou et al., 2005; Weckerle et al., 2011). The overall pathogenic effect of IFN-I signaling in murine SLE has been demonstrated (Agrawal et al., 2009; Santiago-Raber et al., 2003), although in some cases it appears independent of autoAb production (Buechler et al., 2013). Furthermore, both the target cells of IFN-I signaling and the IFN-I-producing cell types in autoAb responses are poorly understood. Plasmacytoid dendritic cells (pDCs) are efficient producers of IFN-I that promote SLE pathogenesis (Rowland et al., 2014; Sisirak et al., 2014). However, other cell types such as stromal follicular dendritic cells (Das et al., 2017) or B cells themselves (Hamilton et al., 2017) have been proposed as IFN-I producers in SLE. Given the emerging therapeutic strategies to block IFN-I in SLE (Muskardin and Niewold, 2018), the precise cellular sources and mechanisms of IFN-I activity in anti-dsDNA responses warrant clarification.

Aberrant immune activation via innate pathways of nucleic acid (NA) sensing plays a fundamental role in SLE. The key extracellular NA sensing pathway involves MyD88-dependent endosomal Toll-like receptors TLR7 and TLR9 that recognize singlestranded RNA and unmethylated DNA, respectively. Both receptors are expressed in B cells and pDCs and facilitate autoAb production and IFN-I secretion by these respective cell types in response to endogenous NAs (Barrat et al., 2005; Leadbetter et al., 2002). TLR7 is necessary for autoreactivity in all tested models and its aberrant expression facilitates SLE in mice and humans (Celhar et al., 2012). The loss of TLR9 reduces anti-nucleosome Abs, yet exacerbates the disease in some SLE models, suggesting a net tolerogenic effect of this receptor (Christensen and Shlomchik, 2007; Sharma et al., 2015). These results remain to be reconciled with the activation of IFN-I production in human pDCs by extracellular DNA via TLR9 (Barrat and Su, 2019), and pose a fundamental question about the innate mechanisms driving anti-DNA responses in SLE.

DNASE1L3 is a secreted DNase that is a critical gatekeeper of tolerance to DNA. Homozygous null mutations in *DNASE1L3* cause rare familial forms of SLE with anti-dsDNA Ab responses (Al-Mayouf et al., 2011; Ozcakar et al., 2013). Furthermore, a coding polymorphism that reduces DNASE1L3 activity is associated with SLE, scleroderma and arthritis (Westra et al., 2018; Zochling et al., 2014). Finally, *Dnase1l3*$^{-/-}$ mice develop rapid and specific anti-dsDNA responses, followed by generalized immune activation and SLE-like disease (Sisirak et al., 2016; Weisenburger et al., 2018). DNASE1L3 acts extracellularly to reduce the availability of antigenic cell-free DNA, e.g. by restricting DNA length (Serpas et al., 2019) and reducing its exposure on apoptotic cell microparticles (Sisirak et al., 2016). Thus, *Dnase1l3*$^{-/-}$ mice represent a clinically relevant model of anti-dsDNA responses driven by extracellular DNA, in which these responses can be studied independently of other autoAbs, lymphoproliferation or systemic inflammation.

Here we took advantage of the specificity and defined kinetics of this model to address the cellular and molecular basis of dsDNA-specific Ab responses. We identified a central role of CD40L-dependent ExFO differentiation in anti-DNA reactivity, and established pDC-derived IFN-I as an important signal for its maintenance. We also found that TLR9 promoted anti-DNA responses and the resulting pathology, and this effect was partially redundant with

TLR7. Thus, extracellular self-DNA drives TLRdependent IFN-I production and continuous ExFO differentiation of antibody-forming cells (AFCs) that drive anti-DNA autoreactivity and pathology in SLE.

Results

Anti-DNA reactivity and autoimmunity in Dnase1l3-deficient mice require CD40L

To test whether rapid anti-nucleosome (anti-Nuc) and anti-dsDNA responses in *Dnase1l3*$^{-/-}$ mice (Sisirak et al., 2016) depend on T cell help via CD40 ligand (CD40L)-CD40 signaling (Lesley et al., 2006), we deleted *Cd40lg* in *Dnase1l3*$^{-/-}$ mice. While *Dnase1l3*$^{-/-}$ mice developed high titers of anti-dsDNA IgG, *Dnase1l3*$^{-/-}$*Cd40lg*$^{-/-}$ mice did not develop any anti-dsDNA Abs detectable by ELISA or *Crithidia luciliae* immunofluorescence test (CLIFT) (Figures 1A, B). They also did not show reactivity to nuclear antigens in the anti-nuclear Ab (ANA) assay (Figures 1C, D). Accordingly, dsDNA- and Nuc-reactive AFCs in the BM and spleen were undetectable by ELISpot in *Dnase1l3*$^{-/-}$*Cd40lg*$^{-/-}$ mice (Figures 1E, F). Whereas the numbers of mature follicular (FO) B cells were unaffected (Figure S1A), *Dnase1l3*$^{-/-}$*Cd40lg*$^{-/-}$ mice harbored a reduced fraction of IgG^{+} AFC (Figures S1B, C) and lower total IgG titers compared to *Dnase1l3*$^{-/-}$ mice, although they were similar to those in wild-type (WT) mice (Figure S1D). However, unlike total IgG responses, anti-DNA AFCs and Abs were completely abrogated (Figures 1A, 1B, 1E and S1B).

Consistent with disrupted CD40L signaling, the fractions of CD62L^{-}CD44^{hi} effector CD4^{+} T cells were significantly lower while those of naïve CD62^{+}CD44^{-}CD4^{+} T cells were higher in *Dnase1l3*$^{-/-}$*Cd40lg*$^{-/-}$ compared to WT and *Dnase1l3*$^{-/-}$ mice (Figure 1G). In parallel, the frequency of CD4^{+}CD25^{hi}Foxp3^{+} regulatory T cells (Tregs) was significantly reduced in *Dnase1l3*$^{-/-}$*Cd40lg*$^{-/-}$ mice (Figure S1E). As expected, GC B cells were completely absent in *Dnase1l3*$^{-/-}$*Cd40lg*$^{-/-}$ mice (Figures S1F, G), and GC-Tfh cells were also reduced (Figure S1H). Notably, *Dnase1l3*$^{-/-}$*Cd40lg*$^{-/-}$ mice lost manifestations of generalized immune activation such as progressive expansion of Ly6C^{-} monocytes in the blood (Figure 1H) and splenomegaly (Figure S1I). *Dnase1l3*$^{-/-}$ mice on the C57BL/6 (B6) background do not develop overt glomerulonephritis but have enlarged glomeruli at 1 year of age (Sisirak et al., 2016). We observed a complete restoration to normal glomerular size in *Dnase1l3*$^{-/-}$*Cd40lg*$^{-/-}$ mice (Figures 1I, J). Thus, anti-dsDNA responses and all disease manifestations in *Dnase1l3*$^{-/-}$ mice require CD40-CD40L signaling, suggesting a strict T cell dependence and revealing the primary role of autoAbs in this model of SLE-like disease.

Germinal center formation is dispensable for autoreactivity

Spontaneous formation of GC in the absence of infection or immunization requires TLR7, whose deletion abolishes GC formation and autoreactivity in several models of autoimmunity (Jackson et al., 2014; Soni et al., 2014). To test whether the T cell-dependent anti-dsDNA response requires GC formation, we generated *Dnase1l3*$^{-/}$*Tlr7*$^{-/-}$ mice. The absence of TLR7 in both WT and *Dnase1l3*$^{-/-}$ mice significantly reduced the fraction of GC B cells and GC formation in the spleen (Figures 2A, B). Despite the loss of GCs, *Dnase1l3*$^{-/-}$*Tlr7*$^{-/-}$ mice accumulated anti-dsDNA and anti-Nuc Abs (Figures 2C, D) and AFC (Figures 2E, F) comparably to GC-sufficient *Dnase1l3*$^{-/-}$ mice. *Dnase1l3*$^{-/-}$*Tlr7*$^{-/-}$

mice also showed positive ANA with a characteristic perinuclear and homogeneous staining pattern (Figures 2G–I), and characteristic kinetoplast staining specific for dsDNA by CLIFT (Figure 2J). Accordingly, TLR7 deficiency did not rescue splenomegaly in old *Dnase1l3*$^{-/-}$ mice (Figure 2K).

We tested whether anti-dsDNA Abs in *Dnase1l3*$^{-/-}$ *Tlr7*$^{-/-}$ mice might be produced by GC B cells residing in the lymph nodes (LN). Unlike spleens, LNs of *Dnase1l3*$^{-/-}$ *Tlr7*$^{-/-}$ mice harbored a substantial number of GC B cells (Figure S2A), as well as total class-switched IgG^{+} B cells (Figure S2B). However, dsDNA and Nuc-reactive AFCs were virtually absent from the LN of both *Dnase1l3*$^{-/-}$ or *Dnase1l3*$^{-/-}$ *Tlr7*$^{-/-}$mice (Figures S2C, D), suggesting that the bulk of autoreactive AFCs were generated in the spleen. Thus, the ablation of TLR7-dependent GC formation does not affect anti-dsDNA responses in *Dnase1l3*$^{-/-}$ mice, arguing against a major role of the GC pathway in this process.

Autoreactivity is driven by extrafollicular B cell differentiation

Given that DNA-specific AFCs were abundant in the spleens of *Dnase1l3*$^{-/-}$ mice, we stained spleen sections for markers of GCs (GL7), plasmablasts (PB) and plasma cells (CD138), and macrophages bordering the follicular areas (CD169). In WT spleens, small clusters of CD138^{+} cells were localized near the bridging channels between the follicular and marginal zones (Figures 3A). In contrast, *Dnase1l3*$^{-/-}$ mice showed an expansion of CD138^{+} cells outside of the follicular areas (Figures 3A and S3A). By flow cytometry, we noted a two-fold increase in the fraction of CXCR3^{+}MHCII^{hi} AFC (Shi et al., 2015) amongst CD138^{+} B cells in *Dnase1l3*$^{-/-}$ splenocytes; these cells were almost undetectable in the absence of CD40L (Figures S3B and 3B). To target the proliferative PB rather than long-lived plasma cells, we treated *Dnase1l3*$^{-/-}$ mice with cyclophosphamide or PBS for 3 days. Four days later, mice were injected with thymidine analogue 5-ethynyl-2’-deoxyuridine (EdU) to label proliferating cells and examined 12 hours later. Cyclophosphamide treatment significantly reduced the fractions of total EdU^{+}, CD138^{+} PB and GL7^{+}CD38^{-} GC B cells among total B cells (Figure S3C). Notably, cyclophosphamide caused a major reduction in splenic dsDNA-and Nuc-specific AFCs (Figure 3C), and a similarly significant reduction in anti-dsDNA and anti-Nuc Ab titers (Figure 3D) and ANA staining (Figure S3D). We also treated *Dnase1l3*$^{-/-}$ mice with a B cell-depleting Ab (anti-CD20), which rapidly reduced FO B cells but spared CD138^{+} PB and GC B cells (Figure S3E, F). Depletion of naïve B cells significantly reduced anti-dsDNA and anti-Nuc Abs only by 4 weeks post-treatment (Figure 3E), consistent with the depletion of B cells as a source of PB. Finally, ELISpot analysis of sorted B cell populations showed that dsDNA- and Nuc-specific AFCs were present only among CD138^{+} PB (Figure 3F), suggesting these short-lived cells as the primary source of autoreactivity.

To gain insight into the receptor repertoire of B cell fractions in *Dnase1l3*$^{-/-}$ mice, we sorted FO, GC, PB and total IgG^{+} B cells individually from two *Dnase1l3*$^{-/-}$ mice (Figures S3G, H) and one age- and sex-matched WT mouse, and sequenced in bulk immunoglobulin heavy chain variable regions (V_H). Complementarity-determining regions (CDRs) of DNA-reactive hybridomas are enriched for positively charged amino acids arginine (Arg) and lysine (Lys), reflecting the binding to negatively charged DNA (Radic and Weigert, 1994). Indeed, the

overall V_H repertoire from PB, GC and IgG^+ fractions from both *Dnase1l3*$^{-/-}$ mice had a 2–3-fold higher frequency of Arg and Lys in the CDRH3 region (Figure 3G). Among V_H families, B cells from *Dnase1l3*$^{-/-}$ mice showed increased utilization of V_H1–5 (Figure 3H), V_H5–17 (Figure 3I) and V_H1–81 (data not shown). The recurrent usage of V_H5–17 was previously noted in anti-dsDNA hybridomas from a different *Dnase1l3*$^{-/-}$ strain (Weisenburger et al., 2018), warranting its further analysis. V_H5–17 clonotypes contained more Arg and Lys residues in the CDRH3 region specifically in the PB of both *Dnase1l3*$^{-/-}$ mice (Figure S3I). Furthermore, in all fractions, the mean CDRH3 isoelectric point and mean CDRH3 hydrophobicity (Kyte-Doolittle index) were higher for the V_H5–17 clonotypes in *Dnase1l3*$^{-/-}$ mice (Figures 3J and S3J). SHM in the V_H regions were not notably higher in any of the B cell fractions from *Dnase1l3*$^{-/-}$ mice, and no dominant clones were observed (Figure S3K and data not shown). Similar to V_H5–17, CDRH3 of V_H1–5 clonotypes from PB and GC fractions of *Dnase1l3*$^{-/-}$ but not WT contained more positively charged amino acids (Figure S3L), supporting the involvement of V_H5–17 and V_H1–5 clones in DNA binding. Collectively, the observed selection for positive charges across all CDRH3 and within particular V_H families suggests a polyclonal expansion of DNA-reactive B cells in *Dnase1l3*$^{-/-}$ mice. The expansion was observed in PB as well as in GC and did not involve extensive SHM typically associated with GC reaction, further supporting short-lived PBs as a source of anti-dsDNA reactivity in *Dnase1l3*$^{-/-}$ mice.

Given the T cell-dependent anti-dsDNA B cell response in *Dnase1l3*$^{-/-}$ mice, we analyzed ExFO-Th cells ($CD62L^-$ $PSGL\text{-}1^{lo}$ $CXCR4^{hi}$ $ICOS^{hi}$) (Figure S3M) and found that this population expanded with age in *Dnase1l3*$^{-/-}$ mice (Figure 3K) in a CD40L-dependent manner (Figure 3L, M). ExFO Th cells showed the highest expression of CXCR4, CD40L and ICOS compared to total T cells or $CD62L^-$ $PSGL\text{-}1^{hi}$ T cells (Figures S3N, O). In addition to their higher frequency (Figure S3P), ExFO Th cells from *Dnase1l3*$^{-/-}$ mice also had significantly higher expression of all three proteins compared to WT (Figures S3N, O). Thus, the expansion of DNA-reactive ExFO AFC in *Dnase1l3*$^{-/-}$ mice is associated with and supported by the expansion of ExFO Th cells. Overall, DNA-specific B cell response appears to proceed through short-lived autoAb-secreting cells with help from T cells in the extrafollicular regions.

IFN-I signaling facilitates extrafollicular anti-dsDNA responses

Given the importance of IFN-I signaling in SLE pathogenesis, we tested its role in ExFO-driven anti-DNA responses by generating *Dnase1l3*$^{-/-}$ *Ifnar1*$^{-/-}$ mice deficient in DNASE1L3 and the IFN-I receptor IFNAR1. The induction of IFN-I-inducible marker Sca-1 on T and B cells (Sisirak et al., 2016) was completely rescued in *Dnase1l3*$^{-/}$ *Ifnar1*$^{-/-}$ mice, confirming a functional blockade of IFN-I signaling (Figures S4A, B). Although *Dnase1l3*$^{-/-}$ *Ifnar1*$^{-/-}$mice showed the initial emergence of anti-dsDNA and anti-Nuc IgG at 1–3 months, the titers were reduced in the majority of animals by 3–6 month and reaching significance at 9–12 month (Figure 4A, B). Accordingly, the numbers of anti-dsDNA and anti-Nuc AFCs at the endpoint were variable but reduced in *Dnase1l3*$^{-/}$ *Ifnar1*$^{-/-}$ mice, reaching significance for anti-dsDNA (Figures 4C, D). The reduction in anti-dsDNA reactivity was also observed by CLIFT (Figure S4C). Moreover, the frequency of total class-switched IgD^- IgM^- $IgG2a.2b^+$ B cells, but not of GC B cells, was significantly reduced in

Dnase1l3$^{-/-}$ *Ifnar1*$^{-/-}$ spleens (Figures S4D, E). Overall ANA reactivity was also significantly reduced in *Dnase1l3*$^{-/-}$ *Ifnar1*$^{-/-}$ mice, with more samples showing reactivity to cytoplasmic antigens (Figures 4E, F). Accordingly, all features of immune activation and pathology were abolished in *Dnase1l3*$^{-/-}$ *Ifnar1*$^{-/-}$ mice, including splenomegaly (Figure S4F), T cell activation (Figure S4G), expansion of Ly6C^{-} monocytes (Figure S4H), the deposition of IgG and complement (C3) in the kidney glomeruli and the increase in glomerular size (Figure 4G–K). Thus, IFN-I signaling appears dispensable for the initial breach of tolerance to DNA, but facilitates the amplification of anti-DNA responses and their downstream pathogenic sequelae.

Consistent with reduced anti-DNA responses, spleens of *Dnase1l3*$^{-/-}$ *Ifnar1*$^{-/-}$ mice showed an overall decrease of CD138^{+} PB in the extrafollicular regions (Figures 5A, B), with a significant reduction of CXCR3^{+} MHC-II^{hi} CD138^{+} PB (Figure 5C, D). Accordingly, the frequency of ExFO Th cells was significantly reduced in *Dnase1l3*$^{-/-}$ *Ifnar1*$^{-/-}$ mice (Figures 5E, F), and the elevated expression of ICOS and CD40L on these cells was completely rescued (Figures 5G,H). *Dnase1l3*$^{-/-}$ mouse spleens harbored multiple CD4^{+} T cells in close proximity with CD138^{+} PB clusters in the red pulp and bridging channels (Figure S5A) and a higher fraction of Ki67^{+} proliferating cells in the GC and T cell zones, with an elevated ratio of proliferating cells to CD4^{+} T cells (Figures 5I–K and S5B). Notably, this ratio was significantly reduced in *Dnase1l3*$^{-/-}$ *Ifnar1*$^{-/-}$ spleens (Figure 5K). Thus, IFN-I is necessary for the maintenance of ExFO B and T cell responses that drive autoreactivity in *Dnase1l3*$^{-/-}$ mice.

Next, we investigated the effect of IFN-I on B cell differentiation into plasmablasts in vitro. Splenic B cells were activated with anti-IgM and anti-CD40 in the presence of IL-4 and increasing doses of IFN-α, which induced a dose-dependent expression of Sca-1 and CD69 on the resulting CD138^{+} PB (Figure S5C, D). A similar pattern of activation and responsiveness to IFN-α was observed between B cells from WT and *Dnase1l3*$^{-/-}$ mice, which were used interchangeably. Purified CFSE-labeled B cells from *Ifnar1*$^{+/+}$ or *Ifnar1*$^{-/-}$ mice were left unactivated (UA) or activated (A) with anti-IgM, anti-CD40 and IL-4 with or without IFN-α for 3 days. The proliferation and differentiation of CFSE-labeled B cells into CD138^{+} PB were comparable between *Ifnar1*$^{+/+}$ and *Ifnar1*$^{-/-}$ mice in the absence of IFN-α, but were increased by IFN-α in IFNAR-proficient B cells (Figure S5E and 5L–O). The enhancing effect of IFN-α was not observed when B cells were stimulated by lipopolysaccharide (LPS) in the presence of IL-4 (Figures S5F, G). Consistent with previous reports (Le Bon et al., 2001; Le Bon et al., 2006), these data suggest that IFN-I may directly facilitate antigen receptor-driven B cell differentiation into PB, supporting the observed role of IFN-I in the ExFO-driven differentiation of autoreactive B cells.

pDCs facilitate extrafollicular anti-dsDNA responses through IFN-I

Having established the role of IFN-I in anti-DNA reactivity in *Dnase1l3*$^{-/-}$ mice, we tested the role of IFN-I-producing pDCs by reducing the dosage of a pDC-specific transcription factor TCF4 (Cisse et al., 2008; Sisirak et al., 2014). *Dnase1l3*$^{-/-}$ *Tcf4*$^{+/-}$ mice on pure 129 background had reduced percentages of pDCs compared to *Tcf4*$^{+/+}$ *Dnase1l3*$^{-/-}$ littermates (Figure S6A), which was also shown to be accompanied by profoundly impaired IFN-I

production (Cisse et al., 2008). As expected, B cell subsets including naïve CD23^{hi} CD21^{lo} FO B cells and CD23^{lo} CD21^{hi} IgM^{hi} marginal zone (MZ) B cells were comparable to the WT (Figures S6B, C). The induction of Sca-1 expression on B and T cells was rescued in *Dnase1l3*$^{-/-}$ *Tcf4*$^{+/-}$ mice (Figures S6D, E), suggesting a global decrease of IFN-I production. Similar to IFNAR1 deficiency, pDC impairment in *Dnase1l3*$^{-/-}$ mice caused a significant reduction of anti-dsDNA and anti-Nuc IgG titers starting at 5–6 months of age (Figures 6A, B). Accordingly, splenic anti-DNA AFCs were also significantly reduced in 1-year-old *Dnase1l3*$^{-/-}$ *Tcf4*$^{+/-}$ mice (Figure 6C), concomitant with reduced expansion of CD138^{+} PB in extrafollicular regions (Figures 6D, H) but normal GC B cell numbers (Figure S6F). *Dnase1l3*$^{-/-}$ *Tcf4*$^{+/-}$ mice also showed a tendency towards reduced ANA; although the effect was variable, ANA pattern showed a higher propensity for dual nuclear and cytoplasmic staining (Figures 6E, I, J). The reduction in anti-dsDNA titers was further confirmed by CLIFT, wherein only 2/7 sera from *Dnase1l3*$^{-/-}$ *Tcf4*$^{+/-}$ mice were positive compared to 5/7 samples from *Dnase1l3*$^{-/-}$ mice at a 1:25 dilution (Figure 6F). A similar reduction of anti-dsDNA titers and a shift towards cytoplasmic ANA staining was observed after the treatment of *Dnase1l3*$^{-/-}$ mice with anti-SiglecH mAb, which inhibits IFN-I production by pDCs (data not shown). All other manifestations of autoimmunity were abolished in *Dnase1l3*$^{-/}$ *Tcf4*$^{+/-}$ mice, including splenomegaly (Figure 6K), T cell activation (Figure S6G), glomerular deposition of C3 and IgG (Figure S6H) and increased size of kidney glomeruli (Figures 6G, L). Overall, pDC impairment by *Tcf4* haplodeficiency phenocopied the loss of IFN-I signaling in *Dnase1l3*$^{-/-}$ mice, suggesting pDCs as the primary source of pathogenic IFN-I.

Immunofluorescent staining of *Dnase1l3*$^{-/-}$ spleens revealed the accumulation of B220^{+} SiglecH^{+} pDCs near the clusters of CD138^{+} B220^{lo-} PB at the border of T cell zones, with frequent juxtaposition of the two cell types (Figure S6I). Although short of a formal proof, these data suggest that some pDCs are located in the extrafollicular region and may directly interact with proliferating plasmablasts. Finally, we activated primary pDCs to produce IFN-α with the TLR9 ligand CpG-A (Figure S6J, K) and tested their effect on B cell differentiation. CFSE-labeled B cells from *Dnase1l3*$^{-/-}$ or *Dnase1l3*$^{-/}$ *Ifnar1*$^{-/-}$ mice were stimulated for 3 days with anti-IgM, anti-CD40 and IL-4 in the absence or presence of CpG-A-stimulated pDCs. CpGA-stimulated pDCs significantly increased the proliferation and differentiation of activated B cells into CD138^{+} SSC^{hi} plasmablasts, and this effect was abolished by IFNAR1 deficiency (Figures 6M, N and S6L, M). We confirmed that IFNAR1 was expressed on activated B cells (Figure S6N), that IFN-α was detectable in the co-culture supernatant only when pDCs were activated with CpG (Figure S6O), and that CD69 was not upregulated on IFNAR1-deficient B cells (Figure S6P). Collectively, these data suggest that pDCs, via the production of IFN-I, directly facilitate anti-DNA responses driven by ExFO B cell differentiation.

Endosomal TLR signaling drives anti-DNA reactivity and SLE-like disease

The observed contribution of pDCs, along with the essential requirement for MyD88-dependent signaling (Sisirak et al., 2016), suggested the role of endosomal TLRs in anti-DNA reactivity. Having excluded the sole contribution of TLR7, we generated *Dnase1l3*$^{-/-}$ *Tlr9*$^{-/-}$ mice deficient in DNASE1L3 and the endosomal DNA sensor TLR9.

Compared to *Dnase1l3*$^{-/-}$ mice, these mice showed only a modest reduction of anti-Nuc Abs but similar titers of anti-dsDNA Abs (Figure 7A, B) and similar numbers of anti-dsDNA and anti-Nuc AFCs (Figure 7C).Furthermore, CXCR3^{+} MHC-II^{hi} CD138^{+} ExFO PB and ExFO Th cells were not reduced in *Dnase1l3*$^{-/-}$ *Tlr9*$^{-/-}$ mice (Figures S7A, B), although a significant reduction of GC B cells was observed (Figure S7C). Total ANA titers in *Dnase1l3*$^{-/-}$ *Tlr9*$^{-/-}$ mice were not reduced (Figures 7D); however, the pattern of ANA reactivity shifted towards cytoplasmic or dual nuclear/cytoplasmic staining (Figure 7E). We also observed a significant decrease in immune activation including splenomegaly (Figure S7D) and expansion of Ly6c^{-} CD11b^{+} myeloid cells (Figures S7E, F). Thus, TLR9 alone is largely dispensable for autoreactivity but contributes to downstream consequences of DNASE1L3 deficiency.

To test whether the contribution of TLR9 might be partially compensated by TLR7, we generated *Dnase1l3*$^{-/-}$ mice deficient in both TLR7 and TLR9 (*Dnase1l3*$^{-/-}$ *Tlr7*$^{-}$ *Tlr9*$^{-/-}$). Unlike *Dnase1l3*$^{-/-}$ *Tlr9* mice, *Dnase1l3*$^{-/-}$ *Tlr7*$^{-}$ *Tlr9*$^{-/-}$ mice completely lost the reactivity to pure dsDNA in the CLIFT assay (Figure 7F), all anti-dsDNA and anti-Nuc reactivity by ELISA (Figures 7G, H), and anti-dsDNA and anti-Nuc AFCs (Figure 7I). This was accompanied by a near-complete loss of ExFo Th cells and of CD138^{+} PB cells expressing CXCR3 (Figures 7J, K), in addition to the expected loss of GC B cells (Figure S7G). Similarly, ANA reactivity was completely abolished (Figures 7L, M), as was splenomegaly (Figure S7H) and the expansion of CD11b^{+}Ly6c^{-} myeloid cells (data not shown). Finally, increased glomerular size (Figure 7N, O) and the glomerular deposition of IgG and C3 (Figure S7I) were fully rescued in *Dnase1l3*$^{-/-}$ *Tlr7*$^{-/-}$ *Tlr9*$^{-/-}$ mice at the endpoint. Notably, these kidney manifestations were partially reduced in *Dnase1l3*$^{-/-}$ *Tlr9*$^{-/-}$and particularly in *Dnase1l3*$^{-/-}$ *Tlr7*$^{-/-}$ mice (Figure 7N, O and Figure S7I), suggesting independent contributions by both TLR9 and TLR7. Altogether, these results reveal essential but partially redundant contributions of TLR9 and TLR7 to autoimmunity driven by extracellular DNA.

Discussion

Dnase1l3$^{-/-}$ mice model the human genetic DNASE1L3 deficiency that results in SLE, and may be relevant for severe sporadic SLE that is frequently associated with reduced extracellular DNase activity (Bruschi et al., 2019). In addition to its clinical relevance, the *Dnase1l3*$^{-/-}$ model manifests prominent anti-dsDNA responses in the absence of additional pathogenetic features such as lymphoproliferation, systemic inflammation or defects of antigen receptor signaling. Importantly, immunopathology in *Dnase1l3*$^{-/-}$ mice comprises three distinct phases: i) initial breach of tolerance to DNA (1–3 months); ii) amplification of anti-DNA Ab responses without reactivity to other self-antigens (3–9 months); iii) spreading of autoreactivity, immune activation and immune complex deposition (9–12 months). This separation of anti-DNA Ab responses from their consequences or other confounding factors make *Dnase1l3*$^{-/-}$ mice an attractive reductionist model of DNA-specific reactivity in SLE.

We found that the ExFO pathway represented the predominant route of autoreactive B cell differentiation in *Dnase1l3*$^{-/-}$ mice, generating short-lived AFCs that produced anti-nucleosome and anti-dsDNA Abs. ExFO B cell responses are generally associated with infections, rapidly generating Abs to protect against pathogens (Cunningham et al., 2007;

Finke et al., 2001). Although the ExFO-generated plasmablasts have been implicated in a lymphoproliferation-driven model of autoreactivity (William et al., 2002), long-lived plasma cells and the GC pathway leading to them are thought to predominate in other models (Degn et al., 2017; Hoyer et al., 2004). Our results do not rule out the role of GC, which may be prominent at late stages of the disease accompanied by broad autoreactivity (Sisirak et al., 2016) and contribute to the generation of pathogenic Abs that synergize with anti-dsDNA Abs to induce renal disease. Furthermore, anti-dsDNA response in *Dnase1l3*$^{-/-}$ mice can be greatly enhanced by additional genetic lesions that cause the expansion of GC (Weisenburger et al., 2018). Collectively, our analysis suggests the ExFO pathway as the primary route of differentiation of DNA-reactive B cells, which continuously generates anti-DNA and can be amplified by additional factors that elicit GC-derived plasma cells.

We found that autoreactivity and inflammation in *Dnase1l3*$^{-/-}$ mice required CD40L signaling and were associated with the expansion of CXCR4^{hi}ICOS^{hi} ExFO-Th cells (Odegard et al., 2008), which was also CD40L-dependent. This is consistent with the role of T cells in general and ExFO-Th cells in particular in other models of ExFO-driven autoreactive responses (Deng et al., 2017; Sweet et al., 2011). Notably, a population of T cells supporting ExFO B cell expansion in human SLE patients has been described recently (Caielli et al., 2019). Together with this and other descriptions of the ExFO B cell differentiation in human SLE (Jenks et al., 2018; Tipton et al., 2015), our data emphasize the predominant role of the ExFO pathway in autoimmunity, including in polyclonal B cell responses driven by DNA. This is consistent with the dynamic nature of anti-dsDNA responses and may also explain the low efficiency of B cell-focused therapies, as these are often inefficient against plasmablasts (Hale et al., 2018). _Indeed, a short 3-day treatment with an anti-proliferative drug cyclophosphamide effectively reduced anti-dsDNA titers, while a month-long treatment with B cell depleting anti-CD20 Ab was required for a similar reduction._Therefore, targeting actively proliferating short-lived plasmablasts in lupus patients with high anti-dsDNA titers represents an important therapeutic goal (Soni and Reizis, 2018).

Given the critical role of IFN-I signaling in SLE pathogenesis and specifically in GC-driven B cell autoreactivity (Domeier et al., 2018), we tested the potential role of this pathway in ExFO-driven anti-dsDNA responses. Our analysis in *Dnase1l3*$^{-/-}$ mice revealed that IFN-I was dispensable for the initial emergence of anti-dsDNA Abs, but facilitated their subsequent maintenance and amplification. Notably, IFN-I was required for the optimal expansion of ExFO CD138^{+} B cells and ICOS^{hi}ExFO-Th cells. These data agree with enhanced generation of short-lived plasmablasts after overexpression of IFN-I in lupus-prone mice (Mathian et al., 2011), and establish the role of endogenous IFN-I in the ExFO pathway. In vitro, IFN-I enhanced B cell differentiation into CD138^{+} plasmablasts that was driven by BCR and CD40 signaling but not by LPS, which presumably mimics B cell responses driven by bacterial pathogens. Thus, continuous activation of self-reactive B cells by antigenic self-DNA, alongside costimulatory signals from T cells, makes B cells responsive to IFN-I-mediated differentiation into AFCs, and therefore may be particularly important for autoAb responses in SLE.

Although the responsiveness of human pDCs to self-DNA (Barrat et al., 2005; Caielli et al., 2016) and the important role of murine pDCs in several SLE models (Rowland et al., 2014; Sisirak et al., 2014) are well established, the mechanism of pDC activity in SLE remains unclear. Furthermore, pDCs appear dispensable in certain models of SLE-like autoreactivity such as Wiskott-Aldrich syndrome deficiency (Sawai et al., 2018). We found that the functional impairment of pDCs phenocopied IFN-I blockade, including the impairment of ExFO-driven anti-DNA responses prior to the abrogation of all downstream pathology. The production of IFN-I by pDCs in vivo has been difficult to detect in this or any other SLE model, likely because of its low and/or transient nature. Nevertheless, in addition to genetic evidence, we were able to show that activated pDCs facilitated CD40-driven plasmablast differentiation in vitro, and this effect was IFN-I-dependent. Together with similar observations for human pDCs in vitro (Jego et al., 2003), these results underscore the emerging role of pDCs as essential IFN-I producers in SLE. They further support antibody-mediated depletion or functional impairment of pDCs as a viable and potentially specific therapeutic strategy in SLE (Barrat and Su, 2019).

Autoreactivity in *Dnase1l3*$^{-/-}$ mice is independent of STING-dependent cytosolic DNA sensing and is completely dependent on MyD88 (Sisirak et al., 2016). We found that the loss of the sole known endosomal DNA receptor, TLR9, had no major effect on anti-dsDNA response as noticed in another Dnase1l3-deficient mouse strain (Weisenburger et al., 2018), and caused a minor albeit significant reduction of immune activation. However, the loss of TLR9 in the absence of TLR7 completely abrogated autoreactivity and pathology, suggesting that TLR9 promoted anti-DNA response yet its pathogenic function was partially compensated by TLR7. The mechanism of such compensation may include a functional competition between the two receptors, whereby TLR9 deletion creates a hyperactive TLR7 (Fukui et al., 2009). This scenario is consistent with the observed shift in autoantibody reactivity by ANA staining pattern as also observed in other SLE models (Christensen et al., 2006; Nickerson et al., 2010). Another possible mechanism includes the ability of TLR7 to recognize both RNA and DNA degradation products such as guanosine and deoxyguanosine, respectively (Shibata et al., 2016). Indeed, the self-antigen in DNASE1L3 deficiency and presumably other SLE forms comprises chromatin in apoptotic microparticles (Nielsen et al., 2011; Pisetsky et al., 2011; Sisirak et al., 2016), which are likely to contain DNA and RNA and their degradation products. Irrespective of the mechanism, the synergistic yet partially redundant role of TLR9 and TLR7 in anti-DNA autoreactivity is consistent with i) the redundancy between the two receptors in an Ab-independent kidney inflammation driven by monocytes (Kuriakose et al., 2019); ii) the requirement for endosomal TLR sensing but not for TLR9 alone in DNA-driven autoimmunity in Dnase2-deficient mice (Pawaria et al., 2015). Our results help reconcile the neutral or even pathogenic effects of deleting TLR9 alone in several SLE models (Celhar et al., 2012; Christensen and Shlomchik, 2007; Sharma et al., 2015) with the emerging pathogenic role of TLR9 in human SLE (Barrat et al., 2005; Caielli et al., 2016). Collectively, our analysis of autoreactivity driven by extracellular DNA supports a prominent role for extrafollicular B cell differentiation into AFCs that requires endosomal TLR signaling and is facilitated by pDCs and IFN-I.

STAR Methods

LEAD CONTACT

Further information and requests for resources and reagents should be directed to and will be fulfilled by the Lead Contact, Boris Reizis (boris.reizis@nyulangone.org).

MATERIALS AVAILABILITY

All animal strains are available from repositories described above. No new animal strains or reagents were generated.

EXPERIMENTAL MODEL DETAILS

Mouse strains—All experiments were performed in accordance with the animal protocol approved by the Institutional Animal Care and use committee of Columbia University and New York University. All the mouse strains were on a C57BL/6 background and C57BL/6J (Stock 000664) mice were used as WT controls unless otherwise mentioned. As described previously (Sisirak et al., 2016), mice with a targeted germline disruption of *Dnase1l3* with *Dnase1L3*^{LacZ} (*Dnase1l3*$^{-/-}$) were purchased from Taconic Animal repository (Model TF2732) and backcrossed onto C57BL/6 or 129SvEvTac for >10 generations and the colonies were maintained in house. Breeding pairs of wild type (WT), *Cd40lg*$^{-/-}$ [002770 - B6.129S2-*Cd40lg*^{tm1Imx}/J], *Tlr7*$^{-/-}$ [008380 – B6.129S1 *Tlr7*^{tm1Flv}/J], *Tlr9*$^{-/-}$ [034329-JAX C57BL/6J-Tlr9^{M7Btlr}/Mmjax] and *Ifnar1*$^{-/-}$ [032045-JAX B6.129S2-*Ifnar1*^{tm1Agt}/Mmjax] mice were purchased from Jackson Laboratories (Bar Harbor, ME) and bred and maintained in house. *Dnase1l3*$^{-/-}$ mice on a pure B6 background were crossed with *Cd40lg*$^{-/-}$, *Tlr7*$^{-/-}$, *Tlr9*$^{-/-}$or *Ifnar1*$^{-/-}$ to generate *Dnase1l3*$^{-/-}$ *Cd40lg*$^{-/-}$, *Dnase1l3*$^{-/-}$ *Tlr7*$^{-/-}$, *Dnase1l3*$^{-/-}$ *Tlr9*$^{-/}$and *Dnase1l3*$^{-/-}$ *Ifnar1*$^{-/-}$ mice respectively. *Dnase1l3*$^{-/-}$ *Tlr7*$^{-/-}$ *and Dnase1l3*$^{-/}$ *Tlr9*$^{-/-}$mice were bred to generate *Dnase1l3*$^{-/-}$ *Tlr7*$^{-/-}$ *Tlr9*$^{-/-}$ triple deficient strain. All the double and triple deficient mice were bred and maintained in house. *Dnase1l3*$^{-/-}$ mice on a pure 129Sv background were crossed with *Tcf4*$^{+/-}$ animals (Zhuang et al., 1996) on pure 129SvEvTac (129Sv) background to generate *Dnase1l3*$^{-/-}$ *Tcf4*$^{+/-}$ mice and bred and maintained in house. 129SvEvTac mice (Taconic farms) were used as WT controls for this cohort.

METHOD DETAILS

Serology: Ig and autoantibody titers—Relative titers of anti-dsDNA, anti-Nucleosome in sera were measured by ELISA. Briefly, Nunc-Immuno maxisorp 96 well flat bottom plates were coated with 50μl/ well of 0.01% poly-L lysine (Sigma Aldrich) for one hour at RT, washed with PBS and coated with 50μl/ well of 10μg/ml calf-thymus DNA (Calbiochem) or 1μg/ml calf-thymus nucleosomes (Arotec diagnostics) in PBS, overnight at 4°C. Excess antigen was washed off using 2–3 washes with PBS. Antigen-coated plates were blocked with 250μl/ well of PBS with 4% non-fat dry milk (NFDM) for 3h at RT. Blocked plates were washed once with PBS and coated with diluted serum in PBS and incubated overnight at 4°C. Unbound serum antibodies were washed off with 3 washes of PBS + 1% NFDM. The bound IgG was detected using a 1:1000 dilution of goat anti-mouse IgG-AP-conjugate (Jackson Immunoresearch) diluted in PBS + 1% NFDM. Unbound

secondary antibody was washed with PBS+ 1% NFDM and developed using diethanolamine substrate buffer (Thermo Fisher Scientific, 34064) and PNPP phosphatase substrate tablets (Sigma Aldrich, SIGMAS0942). For relative quantitation of antigen-specific IgG titers, serum from an anti-DNA or anti-Nuc positive animal was used as a standard using serial double dilutions. O.D. at the lowest serum dilution was arbitrarily assigned a value of 100 U/ml. Standard curve was plotted as O.D. at 405nm vs antigen concentration (U/ml). Relative IgG titers of samples were calculated using the straight-line equation and multiplied with the dilution factor. In all ELISA assays, in each plate, controls and test samples were run together and analyzed using the same standard curve.

Total serum IgG titers were determined by coating the ELISA plates with 5 μg/ml mouse IgG (Southern Biotech) and probing the bound serum antibody with anti-mouse IgG-AP (Jackson Immunoresearch).

ANA analysis—For detection of ANA and assessment of ANA staining patterns, HEp-2 human tissue culture substrate slides (Antibodies Incorporated, Davis, CA) were coated with sera at a 1:50 dilution in PBS for 1h at RT in a hydrated chamber and probed with rat anti-mouse κ- FITC conjugate (Southern Biotechnologies Associates, Birmingham, AL) at a 1:200 dilution. Immunofluorescence images were captured using a Keyence BZ-X710 fluorescence microscope at 20X magnification. The color intensity of images was enhanced slightly using Adobe Photoshop CC (Adobe Systems, San Jose, CA) or ImageJ. This was necessary for better visualization and was carried out consistently between all images while maintaining the integrity of the data. Immunofluorescence intensity was quantitated using ImageJ 1.51s image processing and analysis software (NIH, USA).

Crithidia luciliae* Immunofluorescence test – CLIFT—Crithidia luciliae* is a protozoan routinely used in the clinic as a substrate to specifically detect antibodies to pure dsDNA (without proteins). A positive test shows staining of the kinetoplast of the protozoan, while staining for basal body or nucleus or both without it, is considered a negative test. The substrate was purchased from Euroimmun (Lubeck, Germany). Serum samples from 12-month-old mice were tested at 1:25 dilution. Anti-dsDNA binding was detected using rat anti-mouse Igκ-FITC conjugate (Southern Biotechnologies Associates, Birmingham, AL). Fluorescence images were acquired using a Zeiss Ax10 fluorescence microscope at 63X magnification and processed using ImageJ software.

ELISpot—ELISpot plates (Millipore, Ref# MSIPS4W10; Multiscreen HTS) were coated with 0.01% poly-L lysine for 1h at RT, followed by coating with 100 μg/ ml calf thymus DNA (Sigma Aldrich) or 10 μg/ ml calf thymus nucleosomes (Arotec diagnostics) overnight at 4°C. Blocked with PBS + 5% FCS for 2–3h at RT. Freshly isolated splenocytes or BM cells were resuspended in freshly prepared warm 15% RPMI 1640 media + antibiotics + 1mM L-glutamine at 20×10^6 cells/ ml. 1×10^6 total cells were plated on the top wells and serially double diluted (1:2). ELISpot plates were then incubated for 18h at 37°C with 5% CO_2. Washed with PBS + 1% FCS to remove the cells and probed with a 1:500 dilution of goat anti-mouse IgG AP (Jackson Immunoresearch) for 3–4h at 4°C. After washing, plates were developed using the Vector Blue AP Substrate Kit III (Vector Labs). Spots were captured and counted using ImmunoSpot S6 Analyzer (Cellular Technology Limited, Shaker

Heights, OH). For analysis of total IgG-secreting AFCs, ELISPot plates were coated with goat anti-mouse IgG (SouthernBiotech) at 5μg/ml and blocked with PBS + 5% BSA. Plates were washed with PBS + 1% BSA and probed with a 1:500 dilution of goat anti-mouse IgG AP (Jackson Immunoresearch).

Flow cytometry—Cell suspensions of peripheral blood, mesenteric and inguinal lymph nodes or splenocytes were subjected to red blood cell lysis, washed and resuspended in staining buffer (1% FCS + 2% BSA + 1mM EDTA in PBS). Cells were stained with indicated cell surface markers. For intracellular staining, cells were surface stained and subsequently fixed and permeabilized using FOXP3 intracellular staining kit (eBioscience) and stained with anti-FOXP3-FITC conjugate. EdU positive cells were stained with Click-iT EdU Alexa Fluor 647 Flow cytometry assay kit (Thermo Fisher Scientific # C10424), as per instructions. Samples were acquired using Attune NxT (Thermo Fisher) flow cytometer and analyzed using FLowJo software version 9 or 10 (Tree Star).

Kidney histopathology—For imaging of kidneys, we use at least 4–5 mice per genotype that are closest to the average values of anti-DNA titers and spleen weight for that genotype. One half from each kidney was fixed with 10% neutral formalin for 24h at RT, and stored in 75% ethanol and subsequently embedded in paraffin. 5 μm thick sections were stained with Hematoxylin and Eosin and captured using the PerkinElmer Vectra multispectral imaging system at 40X magnification and glomerular size was analyzed using Slidepath software (Leica Biosystems digital image hub).

Immunofluorescence analysis of kidney and spleen sections—For imaging of the spleens and kidneys we use at least 4–5 mice per genotype that are closest to the average values of anti-DNA titers and spleen weight for that genotype. One half from both kidneys were frozen in OCT (Tissue Tek). 5–10 μm thick kidney sections were fixed using chilled acetone for 10 min. Sections were stained with DAPI, goat anti-mouse IgG-PE conjugate (eBioscience) and goat anti-mouse C3-FITC conjugate (Immunology consultant's Laboratory Inc., Oregon). Images were captured using Keyence BZ-X710 fluorescence microscope at 40X magnification. Immunofluorescence intensity was quantitated using ImageJ 1.51s image processing and analysis software (NIH, USA). The color intensity of images was enhanced slightly using Adobe Photoshop CC (Adobe Systems, San Jose, CA). This was necessary for better visualization and was carried out consistently on whole images of control and test sections.

Spleen were either frozen in OCT and then sectioned and fixed using chilled acetone or were fixed in 4% PFA overnight followed by 8–10 hours of dehydration in 30% sucrose, after which they were frozen in OCT for cryosectioning. 5–10 μm thick spleen sections were stained with indicated anti mouse Ab-conjugates: GL-7-FITC, IgDAPC, CD138-PE, CD169-APC, Ki67-PE, CD4-FITC/ APC, SiglecH-APC and B220-FITC. Images were captured using Keyence BZ-X710 fluorescence microscope at 4X or 20X magnification or using the Zeiss 880 confocal microscope, maintained by NYU Langone Health's Microscopy Laboratory. Scanning of whole sections was achieved using ZEN imaging software– tile and stitch functions. All images were acquired with similar functions. Image analysis was done using Bitplane's Imaris version 9.2.0. Quantification of in situ mean

fluorescence intensity sum of CD138 staining was determined using isosurfacing function with subtraction of background staining of spleen capsule. Quantitative analysis of total number of $CD138^+$ or $Ki67^+$ spots per half spleen represented, were calculated by rendering $CD138^+$ or $Ki67^+$ cells with spots using Imaris image analysis software.

Cyclophosphamide treatment—Ten 6-mo-old *Dnase1l3*$^{-/-}$ mice were bled on day 0 to get pretreatment serum titers of anti-dsDNA and anti-Nucleosome antibodies. 5 mice each were subsequently injected intraperitonially with equal volume of either PBS or 500μg cyclophosphamide monohydrate (CYTOPAC, Sigma Aldrich) reconstituted in PBS per mouse for three consecutive days. Mice were rested for 4 days. Subsequently mice were treated with 1 mg EdU (Carbosynth) intravenously for 12 h after which they were euthanized.

Anti-CD20 treatment—Serum was collected from five-month-old *Dnase1l3*$^{-/-}$ female mice (pretreatment). Subsequently they were injected (i.p) with 100μg of anti-mouse CD20 (clone 5D2), a kind gift from Genentech, or an IgG2a isotype control antibody (C1.18.4, Bio × cell, cat # BE0085), ~ every 15 days for a month. Serum was collected after two weeks of each treatment. Mice were euthanized at six-months of age and spleen was analyzed for AFCs and cellular populations.

Sorting of B cell subsets—Plasmablasts (PB): $CD19^+$ $B220^{+/-}$ $SiglecH^-$ $TCRb^-$ $CD138^{hi}$; Germinal center B cells (GC): $CD19^+$ $B220^+$ $SiglecH^-$ $TCRb^-$ $CD138^-$ $CD38^-$ $GL\text{-}7^{hi}$; Naïve Follicular B cells (FO): $CD19^+$ $B220^+$ $SiglecH^-$ $TCRb^-$ $CD138^-$ $CD38^+$ $GL\text{-}7^-$ $CD44^-$ $Sca1^-$; Follicular activated B cells (FOA): $CD19^+$ $B220^+$ $SiglecH^-$ $TCRb^-$ $CD138^-$ $CD38^+$ $GL\text{-}7^-$ $CD44^{hi}$ $Sca1^{hi}$ and class-switched B cells (IgG^+): $CD19^+$ $B220^+$ $SiglecH^-$ $TCRb^-$ IgD^- IgM^- $IgG2a/2b^+$ were sorted from total splenocytes of > 6 mo old WT or *Dnase1l3*$^{-/-}$ mice using the BD FACSAria III Sorter. Sorted cells were used for ELISPot analysis or BCR repertoire analysis.

BCR sequencing and analysis

VH Sequencing.: Sorted B cell subsets FO, PB, GC and IgG^+ were lysed in TRIzol® Reagent (Invitrogen) and total RNA was extracted and purified using the RNeasy Mini Kit (Qiagen). cDNA was synthesized from 500 ng total RNA using the SuperScript™ IV First-Strand Synthesis System (Invitrogen). Variable heavy (VH) transcript was amplified with a multiplex primer set (primer details in table 1) using FastStart™ High Fidelity PCR System (Roche) under the following conditions: 2 min at 95C; 4 cycles of 92C for 30 s, 50C for 30 s, 72C for 1 min; 4 cycles of 92C for 30 s, 55C for 30 s, 72C for 1 min; 22 cycles of 92C for 30 s, 63C for 30 s, 72C for 1 min; 72C for 7 min; hold at 4C, and sequenced by 2×300 paired-end Illumina MiSeq.

Bioinformatic Analysis.: Raw 2×300 reads were trimmed depending on sequence quality using Trimmomatic (Bolger et al., 2014) and annotated using MiXCR (Bolotin et al., 2015). Sequences with ≥ 2 reads were grouped into clonotypes by clustering those with ≥ 95% CDR-H3 amino acid identity (Edgar, 2010). CDR-H3 characteristics were analyzed using custom Python scripts.

Statistics.: p-values for the analysis of positively charged amino acids within the CDR-H3 and V-gene usage were determined using Fisher's Exact test. p-values for the analysis of the mean CDR-H3 isoelectric point and hydrophobicity were determined using Student's *t*-test or Mann-Whitney *U* test.

In vitro B cell proliferation/ differentiation assay—Naïve B cells were MACS-purified by negative selection from splenocytes of WT, *Dnase1l3*$^{-/-}$, *Ifnar1*$^{-/-}$ or *Dnase1l3*$^{-/-}$ *Ifnar1*$^{-/-}$ mice using CD43 microbeads. Purified B cells were labelled with 3 μM Cell trace CFSE (Invitrogen), in PBS+ 2% BSA for 10 mins at RT. CFSE labelled cells were washed twice with PBS and subsequently suspended in RPMI + 10% FBS + 2mM L-glutamine + 10μM β-Mercaptoethanol and plated in round bottom 96 well plates at a concentration of 0.5×10^6 cells/ well in 200μl media. Cells were either left unactivated or activated with: (1) 5 μg/ml anti-IgM (Jackson Immunoresearch) + anti-CD40 (LEAF-purified, BioLegend) and 5 ng/ml recombinant mouse IL-4 (R&D systems) OR (2) 1μg/ml LPS (LPS-EK Ultrapure, InvivoGen) + 5 ng/ml recombinant mouse IL-4. Unactivated (UA) and activated (A) B cells were supplemented or not with recombinant mouse IFNα1 (BioLegend) at indicated concentrations. B cells were analyzed for activation, proliferation and differentiation after 3 days of culture.

pDC purification—RBC lysed splenocytes or bone marrow cells of *Dnase1l3*$^{-/-}$ mice were resuspended in RPMI + 10% FCS and were allowed to adhere to sterile tissue culture treated 100 mm petriplates for 1h at 37°C after which adherent cells were discarded. Floating cells were resuspended at 10×10^6 cells in 90μl of wash buffer and labelled with the following cocktail of biotinylated antibodies: Anti-IgG, anti-IgM, anti-IgD, anti-CD19, anti-CD93, anti-CD5, anti Ly6G, anti-Ter119, anti-CD41, anti NK1.1, anti-TCRb, anti CD3, anti CD11b, anti-CD24 and anti-F4/80 each at 1: 200 dilution for 20 mins at 4°C. Labeled cells were washed and stained with Streptavidin microbeads for 20 mins at 4°C. Unlabeled cells were collected by negative selection. Up-to 45–50% pure pDCs ($B220^{lo}$ $SiglecH^{+}$ $CD11c^{lo}$) could be routinely identified by flow cytometry.

pDC, B cell co-culture assay—pDCs were purified from *Dnase1l3*$^{-/-}$ BM cells using MACS negative selection (described above) and B cells were purified from *Dnase1l3*$^{-/}$ or *Dnase1l3*$^{-/-}$ *Ifnar1*$^{-/-}$ mice by negative selection using CD43 microbeads and were labeled with cell trace CFSE. 0.5×10^6 purified B cells per well were left unactivated (UA) or activated (A) with 5 μg/ml anti-IgM (Jackson Immunoresearch) + anti-CD40 (BioLegend) and 5 ng/ml recombinant mouse IL-4 (R&D systems). Activated B cells were cultured in the presence of ~2×10^4 purified unactivated pDCs (A + pDCs) OR treated with 1μg/ml CpGA (ODN 2216, InvioGen) (A + CpG) OR co-cultured with ~2×10^4 purified pDCs activated with 1μg/ml CpGA (A + pDCs + CpGA). Cells were co-cultured for three days after which B cells were analyzed for activation, proliferation and differentiation by flow cytometry and supernatant was analyzed for IFNα production by ELISA.

IFNα ELISA

Purified BM or splenic pDCs at various concentrations were left unstimulated or stimulated with 1μg/ml CpGA (ODN 2216, InvioGen) for 18h and supernatant was collected.

Supernatants were collected from pDC + B cells cocultures as described above. Secreted IFNα in culture supernatants was measured using mouse IFN-alpha bioluminescence ELISA kit (InvivoGen) following manufacturer's instructions.

QUANTIFICATION AND STATISTICAL ANALYSIS

Comparisons between multiple groups were performed by one-way ANOVA followed by multiple comparisons analysis, Tukey's test, unless otherwise mentioned. Comparisons between two groups were performed by non-parametric student's *t*-test with Mann-Whitney analysis. P values less than or equal to 0.05 were considered significant and significance was assigned according to the following breakdown: *p < 0.05, ** p < 0.01, *** p< 0.001 and **** p< 0.0001. Graph Pad Prism software vs. 7 or 8 was used for all statistical analysis.

DATA AND CODE AVAILABILITY

VH repertoire sequencing data have been deposited in the NCBI SRA database (accession code pending)

Supplementary Material

Refer to Web version on PubMed Central for supplementary material.

Acknowledgements

Supported by the NIH grants AI072571 (B.R.), AR071703 (B.R., G.C.I.), AR070591 (B.R.), CA232666 (O.A.P.), AI100853 (O.A.P., L.S.), AR069515 (L.S.), HL145997 (J.N.P), CA009161 (J.N.P), CA110624 (G.C.I.) and AR071703 (G.C.I.). Also supported by the Lupus Research Alliance (B.R.), the Colton Center for Autoimmunity (B.R.), Idex Junior Chair program from the Bordeaux University (V.S.) and Cancer Research Institute CLIP grant (V.S).

References

Agrawal H, Jacob N, Carreras E, Bajana S, Putterman C, Turner S, Neas B, Mathian A, Koss MN, Stohl W, et al. (2009). Deficiency of type I IFN receptor in lupus-prone New Zealand mixed 2328 mice decreases dendritic cell numbers and activation and protects from disease. J Immunol 183, 6021–6029. [PubMed: 19812195]

Al-Mayouf SM, Sunker A, Abdwani R, Abrawi SA, Almurshedi F, Alhashmi N, Al Sonbul A, Sewairi W, Qari A, Abdallah E, et al. (2011). Loss-of-function variant in DNASE1L3 causes a familial form of systemic lupus erythematosus. Nat Genet 43, 1186–1188. [PubMed: 22019780]

Barrat FJ, Meeker T, Gregorio J, Chan JH, Uematsu S, Akira S, Chang B, Duramad O, and Coffman RL (2005). Nucleic acids of mammalian origin can act as endogenous ligands for Toll-like receptors and may promote systemic lupus erythematosus. J Exp Med 202, 1131–1139. [PubMed: 16230478]

Barrat FJ, and Su L (2019). A pathogenic role of plasmacytoid dendritic cells in autoimmunity and chronic viral infection. J Exp Med.

Bennett L, Palucka AK, Arce E, Cantrell V, Borvak J, Banchereau J, and Pascual V (2003). Interferon and granulopoiesis signatures in systemic lupus erythematosus blood. J Exp Med 197, 711–723. [PubMed: 12642603]

Bolger AM, Lohse M, and Usadel B (2014). Trimmomatic: a flexible trimmer for Illumina sequence data. Bioinformatics 30, 2114–2120. [PubMed: 24695404]

Bolotin DA, Poslavsky S, Mitrophanov I, Shugay M, Mamedov IZ, Putintseva EV, and Chudakov DM (2015). MiXCR: software for comprehensive adaptive immunity profiling. Nat Methods 12, 380–381. [PubMed: 25924071]

Bruschi M, Bonanni A, Petretto A, Vaglio A, Pratesi F, Santucci L, Migliorini P, Bertelli R, Galetti M, Belletti S, et al. (2019). Neutrophil Extracellular Traps (NETs) profiles in patients with incident SLE and lupus nephritis. J Rheumatol.

Buechler MB, Teal TH, Elkon KB, and Hamerman JA (2013). Cutting edge: Type I IFN drives emergency myelopoiesis and peripheral myeloid expansion during chronic TLR7 signaling. J Immunol 190, 886–891. [PubMed: 23303674]

Caielli S, Athale S, Domic B, Murat E, Chandra M, Banchereau R, Baisch J, Phelps K, Clayton S, Gong M, et al. (2016). Oxidized mitochondrial nucleoids released by neutrophils drive type I interferon production in human lupus. J Exp Med.

Caielli S, Veiga DT, Balasubramanian P, Athale S, Domic B, Murat E, Banchereau R, Xu Z, Chandra M, Chung CH, et al. (2019). A CD4(+) T cell population expanded in lupus blood provides B cell help through interleukin-10 and succinate. Nat Med 25, 75–81. [PubMed: 30478422]

Celhar T, Magalhaes R, and Fairhurst AM (2012). TLR7 and TLR9 in SLE: when sensing self goes wrong. Immunol Res 53, 58–77. [PubMed: 22434514]

Christensen SR, and Shlomchik MJ (2007). Regulation of lupus-related autoantibody production and clinical disease by Toll-like receptors. Semin Immunol 19, 11–23. [PubMed: 17276080]

Christensen SR, Shupe J, Nickerson K, Kashgarian M, Flavell RA, and Shlomchik MJ (2006). Toll-like receptor 7 and TLR9 dictate autoantibody specificity and have opposing inflammatory and regulatory roles in a murine model of lupus. Immunity 25, 417–428. [PubMed: 16973389]

Cisse B, Caton ML, Lehner M, Maeda T, Scheu S, Locksley R, Holmberg D, Zweier C, den Hollander NS, Kant SG, et al. (2008). Transcription factor E2–2 is an essential and specific regulator of plasmacytoid dendritic cell development. Cell 135, 37–48. [PubMed: 18854153]

Cunningham AF, Gaspal F, Serre K, Mohr E, Henderson IR, Scott-Tucker A, Kenny SM, Khan M, Toellner KM, Lane PJ, and MacLennan IC (2007). Salmonella induces a switched antibody response without germinal centers that impedes the extracellular spread of infection. J Immunol 178, 6200–6207. [PubMed: 17475847]

Das A, Heesters BA, Bialas A, O'Flynn J, Rifkin IR, Ochando J, Mittereder N, Carlesso G, Herbst R, and Carroll MC (2017). Follicular Dendritic Cell Activation by TLR Ligands Promotes Autoreactive B Cell Responses. Immunity 46, 106–119. [PubMed: 28099860]

Degn SE, van der Poel CE, Firl DJ, Ayoglu B, Al Qureshah FA, Bajic G, Mesin L, Reynaud CA, Weill JC, Utz PJ, et al. (2017). Clonal Evolution of Autoreactive Germinal Centers. Cell 170, 913–926 e919. [PubMed: 28841417]

Deng R, Hurtz C, Song Q, Yue C, Xiao G, Yu H, Wu X, Muschen M, Forman S, Martin PJ, and Zeng D (2017). Extrafollicular CD4(+) T-B interactions are sufficient for inducing autoimmune-like chronic graft-versus-host disease. Nat Commun 8, 978. [PubMed: 29042531]

Domeier PP, Chodisetti SB, Schell SL, Kawasawa YI, Fasnacht MJ, Soni C, and Rahman ZSM (2018). B-Cell-Intrinsic Type 1 Interferon Signaling Is Crucial for Loss of Tolerance and the Development of Autoreactive B Cells. Cell Rep 24, 406–418. [PubMed: 29996101]

Edgar RC (2010). Search and clustering orders of magnitude faster than BLAST. Bioinformatics 26, 2460–2461. [PubMed: 20709691]

Finke D, Baribaud F, Diggelmann H, and Acha-Orbea H (2001). Extrafollicular plasmablast B cells play a key role in carrying retroviral infection to peripheral organs. J Immunol 166, 6266–6275. [PubMed: 11342650]

Fukui R, Saitoh S, Matsumoto F, Kozuka-Hata H, Oyama M, Tabeta K, Beutler B, and Miyake K (2009). Unc93B1 biases Toll-like receptor responses to nucleic acid in dendritic cells toward DNA- but against RNA-sensing. J Exp Med 206, 1339–1350. [PubMed: 19451267]

Hale M, Rawlings DJ, and Jackson SW (2018). The long and the short of it: insights into the cellular source of autoantibodies as revealed by B cell depletion therapy. Curr Opin Immunol 55, 81–88. [PubMed: 30390507]

Hamilton JA, Wu Q, Yang P, Luo B, Liu S, Hong H, Li J, Walter MR, Fish EN, Hsu HC, and Mountz JD (2017). Cutting Edge: Endogenous IFN-beta Regulates Survival and Development of Transitional B Cells. J Immunol 199, 2618–2623. [PubMed: 28904124]

Hoyer BF, Moser K, Hauser AE, Peddinghaus A, Voigt C, Eilat D, Radbruch A, Hiepe F, and Manz RA (2004). Short-lived plasmablasts and long-lived plasma cells contribute to chronic humoral autoimmunity in NZB/W mice. J Exp Med 199, 1577–1584. [PubMed: 15173206]

Jackson SW, Scharping NE, Kolhatkar NS, Khim S, Schwartz MA, Li QZ, Hudkins KL, Alpers CE, Liggitt D, and Rawlings DJ (2014). Opposing impact of B cell-intrinsic TLR7 and TLR9 signals on autoantibody repertoire and systemic inflammation. J Immunol 192, 4525–4532. [PubMed: 24711620]

Jego G, Palucka AK, Blanck JP, Chalouni C, Pascual V, and Banchereau J (2003). Plasmacytoid dendritic cells induce plasma cell differentiation through type I interferon and interleukin 6. Immunity 19, 225–234. [PubMed: 12932356]

Jenks SA, Cashman KS, Woodruff MC, Lee FE, and Sanz I (2019). Extrafollicular responses in humans and SLE. Immunol Rev 288, 136–148. [PubMed: 30874345]

Jenks SA, Cashman KS, Zumaquero E, Marigorta UM, Patel AV, Wang X, Tomar D, Woodruff MC, Simon Z, Bugrovsky R, et al. (2018). Distinct Effector B Cells Induced by Unregulated Toll-like Receptor 7 Contribute to Pathogenic Responses in Systemic Lupus Erythematosus. Immunity 49, 725–739 e726. [PubMed: 30314758]

Kirou KA, Lee C, George S, Louca K, Peterson MG, and Crow MK (2005). Activation of the interferon-alpha pathway identifies a subgroup of systemic lupus erythematosus patients with distinct serologic features and active disease. Arthritis Rheum 52, 1491–1503. [PubMed: 15880830]

Kuriakose J, Redecke V, Guy C, Zhou J, Wu R, Ippagunta SK, Tillman H, Walker PD, Vogel P, and Hacker H (2019). Patrolling monocytes promote the pathogenesis of early lupus-like glomerulonephritis. J Clin Invest 129, 2251–2265. [PubMed: 31033479]

Le Bon A, Schiavoni G, D'Agostino G, Gresser I, Belardelli F, and Tough DF (2001). Type i interferons potently enhance humoral immunity and can promote isotype switching by stimulating dendritic cells in vivo. Immunity 14, 461–470. [PubMed: 11336691]

Le Bon A, Thompson C, Kamphuis E, Durand V, Rossmann C, Kalinke U, and Tough DF (2006). Cutting edge: enhancement of antibody responses through direct stimulation of B and T cells by type I IFN. J Immunol 176, 2074–2078. [PubMed: 16455962]

Leadbetter EA, Rifkin IR, Hohlbaum AM, Beaudette BC, Shlomchik MJ, and Marshak-Rothstein A (2002). Chromatin-IgG complexes activate B cells by dual engagement of IgM and Toll-like receptors. Nature 416, 603–607. [PubMed: 11948342]

Lesley R, Kelly LM, Xu Y, and Cyster JG (2006). Naive CD4 T cells constitutively express CD40L and augment autoreactive B cell survival. Proc Natl Acad Sci U S A 103, 10717–10722. [PubMed: 16815973]

Mathian A, Gallegos M, Pascual V, Banchereau J, and Koutouzov S (2011). Interferon-alpha induces unabated production of short-lived plasma cells in preautoimmune lupus-prone (NZBxNZW)F1 mice but not in BALB/c mice. Eur J Immunol 41, 863–872. [PubMed: 21312191]

Muskardin TLW, and Niewold TB (2018). Type I interferon in rheumatic diseases. Nat Rev Rheumatol 14, 214–228. [PubMed: 29559718]

Nickerson KM, Christensen SR, Shupe J, Kashgarian M, Kim D, Elkon K, and Shlomchik MJ (2010). TLR9 regulates TLR7- and MyD88-dependent autoantibody production and disease in a murine model of lupus. J Immunol 184, 1840–1848. [PubMed: 20089701]

Nielsen CT, Ostergaard O, Johnsen C, Jacobsen S, and Heegaard NH (2011). Distinct features of circulating microparticles and their relationship to clinical manifestations in systemic lupus erythematosus. Arthritis Rheum 63, 3067–3077. [PubMed: 21702008]

Odegard JM, Marks BR, DiPlacido LD, Poholek AC, Kono DH, Dong C, Flavell RA, and Craft J (2008). ICOS-dependent extrafollicular helper T cells elicit IgG production via IL-21 in systemic autoimmunity. J Exp Med 205, 2873–2886. [PubMed: 18981236]

Ozcakar ZB, Foster J 2nd, Diaz-Horta O, Kasapcopur O, Fan YS, Yalcinkaya F, and Tekin M (2013). DNASE1L3 mutations in hypocomplementemic urticarial vasculitis syndrome. Arthritis Rheum 65, 2183–2189. [PubMed: 23666765]

Pawaria S, Moody KL, Busto P, Nundel K, Baum R, Sharma S, Gravallese EM, Fitzgerald KA, and Marshak-Rothstein A (2015). An unexpected role for RNA-sensing toll-like receptors in a murine model of DNA accrual. Clin Exp Rheumatol 33, S70–73.

Pisetsky DS (2016). Anti-DNA antibodies--quintessential biomarkers of SLE. Nat Rev Rheumatol 12, 102–110. [PubMed: 26581343]

Pisetsky DS, Gauley J, and Ullal AJ (2011). Microparticles as a source of extracellular DNA. Immunol Res 49, 227–234. [PubMed: 21132466]

Radic MZ, and Weigert M (1994). Genetic and structural evidence for antigen selection of anti-DNA antibodies. Annu Rev Immunol 12, 487–520. [PubMed: 8011289]

Rowland SL, Riggs JM, Gilfillan S, Bugatti M, Vermi W, Kolbeck R, Unanue ER, Sanjuan MA, and Colonna M (2014). Early, transient depletion of plasmacytoid dendritic cells ameliorates autoimmunity in a lupus model. J Exp Med 211, 1977–1991. [PubMed: 25180065]

Santiago-Raber ML, Baccala R, Haraldsson KM, Choubey D, Stewart TA, Kono DH, and Theofilopoulos AN (2003). Type-I interferon receptor deficiency reduces lupus-like disease in NZB mice. J Exp Med 197, 777–788. [PubMed: 12642605]

Sawai CM, Serpas L, Neto AG, Jang G, Rashidfarrokhi A, Kolbeck R, Sanjuan MA, Reizis B, and Sisirak V (2018). Plasmacytoid Dendritic Cells Are Largely Dispensable for the Pathogenesis of Experimental Inflammatory Bowel Disease. Front Immunol 9, 2475. [PubMed: 30410494]

Seo SJ, Fields ML, Buckler JL, Reed AJ, Mandik-Nayak L, Nish SA, Noelle RJ, Turka LA, Finkelman FD, Caton AJ, and Erikson J (2002). The impact of T helper and T regulatory cells on the regulation of anti-doublestranded DNA B cells. Immunity 16, 535–546. [PubMed: 11970877]

Serpas L, Chan RWY, Jiang P, Ni M, Sun K, Rashidfarrokhi A, Soni C, Sisirak V, Lee WS, Cheng SH, et al. (2019). Dnase1l3 deletion causes aberrations in length and end-motif frequencies in plasma DNA. Proc Natl Acad Sci U S A 116, 641–649. [PubMed: 30593563]

Sharma S, Fitzgerald KA, Cancro MP, and Marshak-Rothstein A (2015). Nucleic Acid-Sensing Receptors: Rheostats of Autoimmunity and Autoinflammation. J Immunol 195, 3507–3512. [PubMed: 26432899]

Shi W, Liao Y, Willis SN, Taubenheim N, Inouye M, Tarlinton DM, Smyth GK, Hodgkin PD, Nutt SL, and Corcoran LM (2015). Transcriptional profiling of mouse B cell terminal differentiation defines a signature for antibody-secreting plasma cells. Nat Immunol 16, 663–673. [PubMed: 25894659]

Shibata T, Ohto U, Nomura S, Kibata K, Motoi Y, Zhang Y, Murakami Y, Fukui R, Ishimoto T, Sano S, et al. (2016). Guanosine and its modified derivatives are endogenous ligands for TLR7. Int Immunol 28, 211–222. [PubMed: 26489884]

Sisirak V, Ganguly D, Lewis KL, Couillault C, Tanaka L, Bolland S, D'Agati V, Elkon KB, and Reizis B (2014). Genetic evidence for the role of plasmacytoid dendritic cells in systemic lupus erythematosus. J Exp Med 211, 1969–1976. [PubMed: 25180061]

Sisirak V, Sally B, D'Agati V, Martinez-Ortiz W, Ozcakar ZB, David J, Rashidfarrokhi A, Yeste A, Panea C, Chida AS, et al. (2016). Digestion of Chromatin in Apoptotic Cell Microparticles Prevents Autoimmunity. Cell 166, 88–101. [PubMed: 27293190]

Soni C, and Reizis B (2018). DNA as a self-antigen: nature and regulation. Curr Opin Immunol 55, 31–37. [PubMed: 30261321]

Soni C, Wong EB, Domeier PP, Khan TN, Satoh T, Akira S, and Rahman ZS (2014). B cell-intrinsic TLR7 signaling is essential for the development of spontaneous germinal centers. J Immunol 193, 4400–4414. [PubMed: 25252960]

Sweet RA, Ols ML, Cullen JL, Milam AV, Yagita H, and Shlomchik MJ (2011). Facultative role for T cells in extrafollicular Toll-like receptor-dependent autoreactive B-cell responses in vivo. Proc Natl Acad Sci U S A 108, 7932–7937. [PubMed: 21518858]

Tipton CM, Fucile CF, Darce J, Chida A, Ichikawa T, Gregoretti I, Schieferl S, Hom J, Jenks S, Feldman RJ, et al. (2015). Diversity, cellular origin and autoreactivity of antibody-secreting cell population expansions in acute systemic lupus erythematosus. Nat Immunol 16, 755–765. [PubMed: 26006014]

Vinuesa CG, Linterman MA, Yu D, and MacLennan IC (2016). Follicular Helper T Cells. Annu Rev Immunol 34, 335–368. [PubMed: 26907215]

Vinuesa CG, Sanz I, and Cook MC (2009). Dysregulation of germinal centres in autoimmune disease. Nat Rev Immunol 9, 845–857. [PubMed: 19935804]

Weckerle CE, Franek BS, Kelly JA, Kumabe M, Mikolaitis RA, Green SL, Utset TO, Jolly M, James JA, Harley JB, and Niewold TB (2011). Network analysis of associations between serum interferon-alpha activity, autoantibodies, and clinical features in systemic lupus erythematosus. Arthritis Rheum 63, 1044–1053. [PubMed: 21162028]

Weisenburger T, von Neubeck B, Schneider A, Ebert N, Schreyer D, Acs A, and Winkler TH (2018). Epistatic Interactions Between Mutations of Deoxyribonuclease 1-Like 3 and the Inhibitory Fc Gamma Receptor IIB Result in Very Early and Massive Autoantibodies Against Double-Stranded DNA. Front Immunol 9, 1551. [PubMed: 30026744]

Westra HJ, Martinez-Bonet M, Onengut-Gumuscu S, Lee A, Luo Y, Teslovich N, Worthington J, Martin J, Huizinga T, Klareskog L, et al. (2018). Finemapping and functional studies highlight potential causal variants for rheumatoid arthritis and type 1 diabetes. Nat Genet 50, 1366–1374. [PubMed: 30224649]

William J, Euler C, Christensen S, and Shlomchik MJ (2002). Evolution of autoantibody responses via somatic hypermutation outside of germinal centers. Science 297, 2066–2070. [PubMed: 12242446]

Yung S, and Chan TM (2015). Mechanisms of Kidney Injury in Lupus Nephritis - the Role of Anti-dsDNA Antibodies. Front Immunol 6, 475. [PubMed: 26441980]

Zhuang Y, Cheng P, and Weintraub H (1996). B-lymphocyte development is regulated by the combined dosage of three basic helix-loop-helix genes, E2A, E2–2, and HEB. Mol Cell Biol 16, 2898–2905. [PubMed: 8649400]

Zochling J, Newell F, Charlesworth JC, Leo P, Stankovich J, Cortes A, Zhou Y, Stevens W, Sahhar J, Roddy J, et al. (2014). An Immunochip-based interrogation of scleroderma susceptibility variants identifies a novel association at DNASE1L3. Arthritis Res Ther 16, 438. [PubMed: 25332064]

Highlights

- Anti-DNA antibody response is driven by T-dependent extrafollicular plasmablasts
- IFN-I signaling propagates anti-DNA responses and SLE-like disease
- IFN-I produced by pDCs promotes plasmablast proliferation and differentiation
- TLR9 drives anti-DNA responses and autoimmunity redundantly with TLR7

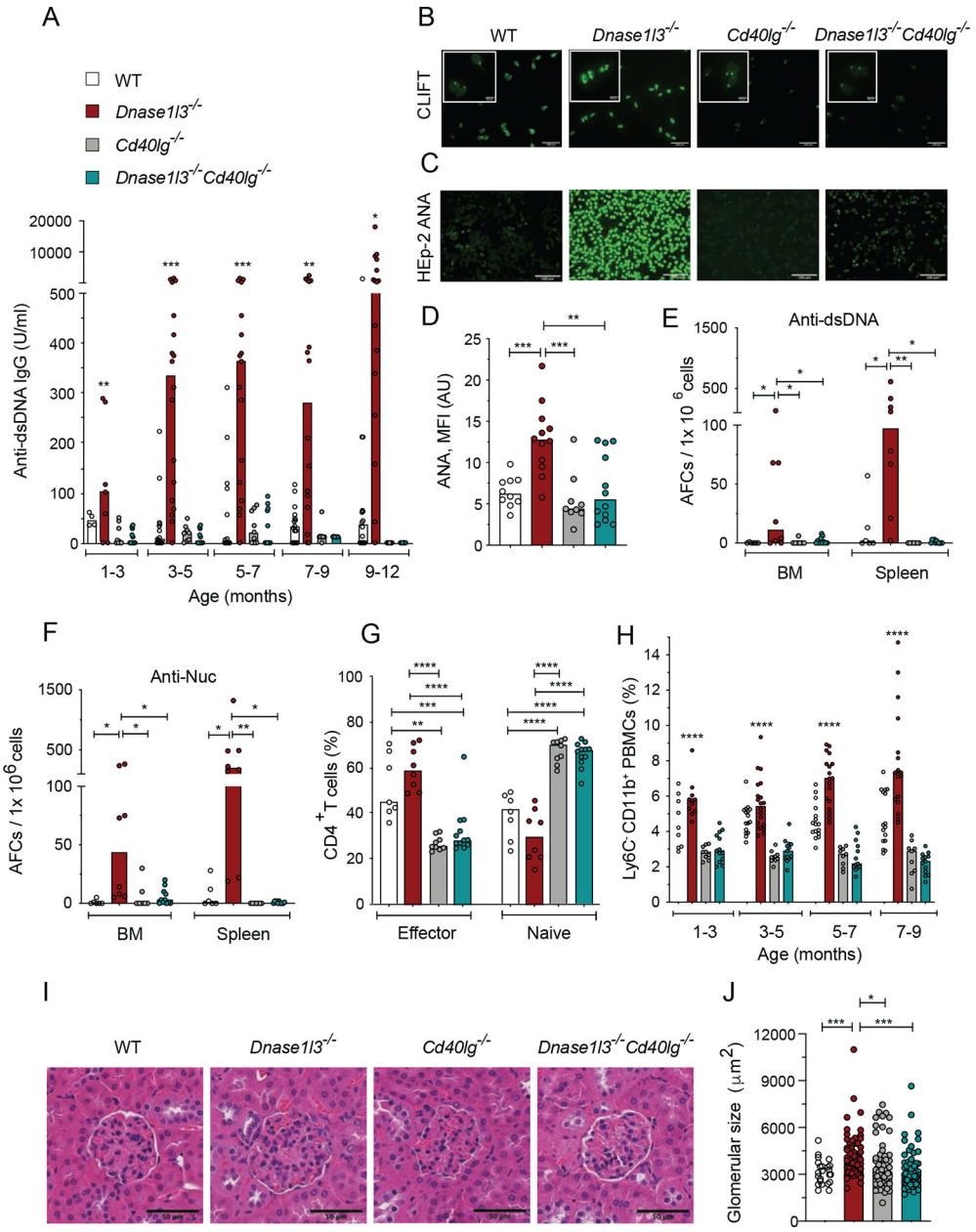

Figure 1. CD40L deficiency in *Dnase1l3*$^{-/-}$ mice abolishes autoimmunity.

Wild-type (WT), *Dnase1l3*$^{-/-}$, *Cd40lg*$^{-/-}$ and *Dnase1l3*$^{-/-}$*Cd40lg*$^{-/-}$ mice were examined for Abs at the indicated ages or at the 12 month endpoint.

(A) Serum anti-dsDNA IgG titers measured by ELISA.

(B) CLIFT assay for anti-dsDNA IgG (representative of ≥4 mice per strain). Arrow indicates positive staining of the kinetoplast. Scale bar, 100 μm (insets, 20 μm).

(C, D) ANA assay, showing images representative of ≥8 mice per strain (C), and quantitation of fluorescence intensity (D). Scale bars, 100μm.

(E, F) Frequency of anti-dsDNA (E) and anti-nucleosome (F) AFCs in the bone marrow (BM) or spleen as determined by ELISpot.

(G) Fractions of effector and naive T cells among splenic CD4^{+} T cells at the endpoint.

(H) Fractions of $CD11b^{+}Ly6c^{-}$ population among total PBMCs at indicated time points.
(I) Glomeruli from H&E-stained kidney sections (representative of ≥3 mice per group). Scale bars, 50 μm.
(J) Size of ≥ 20 glomeruli per kidney section from ≥3 mice per group.
In A and H, significant differences between *Dnase1l3*$^{-/-}$ vs *Dnase1l3*$^{-/-}$*Cd40lg*$^{-/-}$mice are shown. Symbols represent individual mice except in panel J, where they represent individual glomeruli. All bars indicate median.
* $p \leq 0.05$, ** $p \leq 0.01$, ***$p \leq 0.001$ and **** $p \leq 0.0001$.
See also Figure S1.

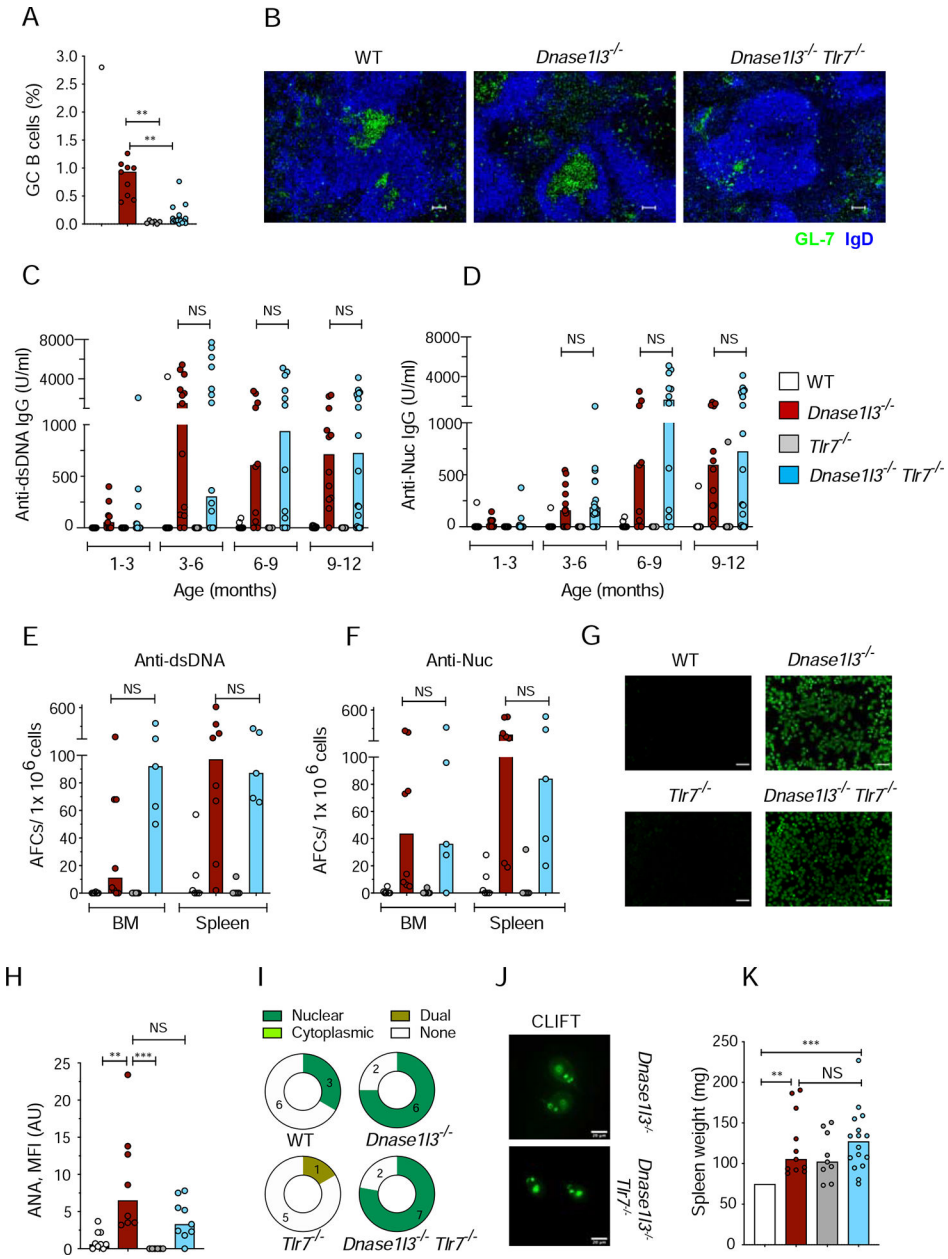

Figure 2. TLR7-deficient *Dnase1l3*$^{-/-}$ mice do not develop germinal centers but retain anti-DNA reactivity.

Wild-type (WT), *Dnase1l3*$^{-/-}$, *Tlr7*$^{-/-}$ and *Dnase1l3*$^{-/-}$ *Tlr7*$^{-/-}$ mice were examined for Abs at the indicated ages or at the 12 month endpoint.

(A) Fraction of CD38^{-} GL-7^{+} GC B cells among splenic B cells at the endpoint.

(B) Spleen sections stained for GC B cells (green) and follicular B cells (blue). Representative of ≥3 mice per group. Scale bars, 30 μm.

(C, D) Serum anti-dsDNA (C), and anti-Nucleosome (Nuc, D) IgG titers measured by ELISA.

(E, F) Frequency of anti-dsDNA (E), and anti-nucleosome (F) AFCs in the bone marrow (BM) or spleen as determined by ELISpot.

(G, H) ANA assay, showing images representative of ≥8 mice per strain (G), and quantitation of fluorescence intensity (H). Scale bars, 100μm.
(I) Distribution of ANA reactivity patterns in mice from each group.
(J) CLIFT assay for anti-dsDNA IgG (representative of ≥4 mice per strain). Scale bar, 20 μm.
(K) Spleen weights at the endpoint.
Symbols represent individual mice; bars indicate median.
NS= not significant, * $p \leq 0.05$, ** $p \leq 0.01$ and *** $p \leq 0.001$
See also Figure S2.

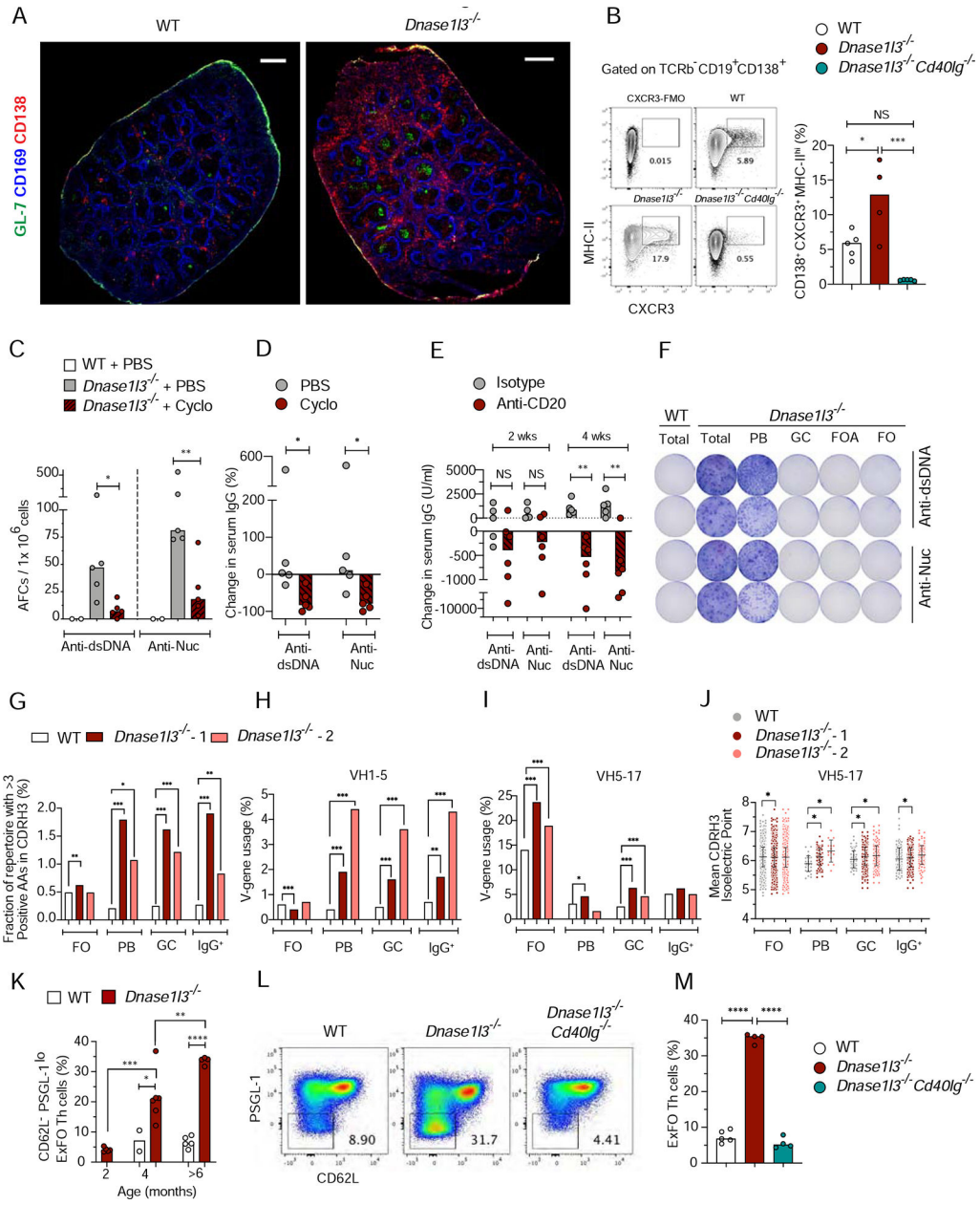

Figure 3. DNA-reactive B cells in *Dnase1l3*$^{-/-}$ mice develop primarily through ExFO differentiation into plasmablasts.

(A) Spleen sections representative of 3–5 WT or *Dnase1l3*$^{-/-}$ mice stained for CD138 (red), CD169 (blue) and GL-7 (green). Scale bar, 1000μm.

(B) Shown are representative flow plots and quantitation of the fraction of CXCR3^{+}MHC-II^{hi} (ExFO) B cells, pre-gated on splenic TCRβ^{-}B220^{+}CD19^{+}CD138^{+} cells from WT (open symbols), *Dnase1l3*$^{-/-}$ (red) and *Dnase1l3*$^{-/-}$*Cd40lg*$^{-/-}$ (green) mice. CXCR3-FMO (fluorescence minus one) was used for gate allocation.

(C, D) Frequency of anti-dsDNA, and anti-nucleosome (Nuc) antibody-forming cells (AFCs), determined by ELISpot (C); and percent change in serum anti-dsDNA or antiNuc

IgG titers determined by ELISA (D), in 6-mo-old WT mice (open) or *Dnase1l3*$^{-/-}$ mice treated with PBS (grey) or cyclophosphamide (cyclo, red).

(E) Change in serum titers of anti-dsDNA or anti-Nuc IgG in 6-mo-old *Dnase1l3*$^{-/-}$ mice after one dose (100μg/ mouse; i.p.) of treatment with IgG2a isotype control (grey) or anti-CD20 Ab (red) at 2 weeks and upon second dose of a similar treatment at 4 weeks.

(F) Image of ELISpot plate representative of 2 experiments with two mice per experiment. Shown are two serial dilutions of anti-dsDNA, and anti-nucleosome (Nuc) antibody-forming cells (AFCs) from total splenocytes of >6-mo-old WT and *Dnase1l3*$^{-/-}$ mice OR from flow sorted – Plasmablasts (PB); Germinal center B cells (GC); Follicular activated B cells (FOA) and Naïve Follicular B cells (FO) from >6 mo old *Dnase1l3*$^{-/-}$ mice. Sorted GC, FOA and FO cells were activated for 2h with 5 μg/ml anti-CD40 + 1 μg/ml LPS, and plated onto DNA or Nuc coated ELISpot plates.

(G) Percentage of clonotypes in each repertoire that contain >3 positively charged amino acids (AA) within the CDR-H3 region, in FO, PB, GC and IgG^{+} B cells from WT (open), *Dnase1l3*$^{-/-}$ −1 (red) and *Dnase1l3*$^{-/-}$ −2 (salmon).

(H, I) Percentage of clonotypes that use the V-gene IGHV1–5 (H), and V-gene IGH5–17 (I) in the indicated B cell subsets and mice.

(J) Mean isoelectric point of the CDR-H3 region among the clonotypes that use the V-gene IGH5–17. Each point represents one clonotype. Error bars represent the mean and S.D. of all clonotypes in each group.

(K) Flow analysis of the fraction of CD62L^{-}PSGL-1^{lo}ExFO Th cells among splenic B220TCRβ^{+}CD4^{+} T cells of WT and *Dnase1l3*$^{-/-}$ mice at the indicated ages.

(L, M) Representative flow plots of pre-gated splenic B220^{-}TCRβ^{+}CD4^{+} cells with low ExFO Th cells shown within the gate (L); quantitation of the fraction of ExFO Th cells (M) from >6-mo-old WT, *Dnase1l3*$^{-/-}$ and *Dnase1l3*$^{-/-}$ *Cd40lg*$^{-/-}$ mice.

For panels A-E, K and M symbols represent individual mice and bars indicate median.

* $p \leq 0.05$, ** $p \leq 0.01$, *** $p \leq 0.001$ and **** $p \leq 0.0001$.

See also Figure S3.

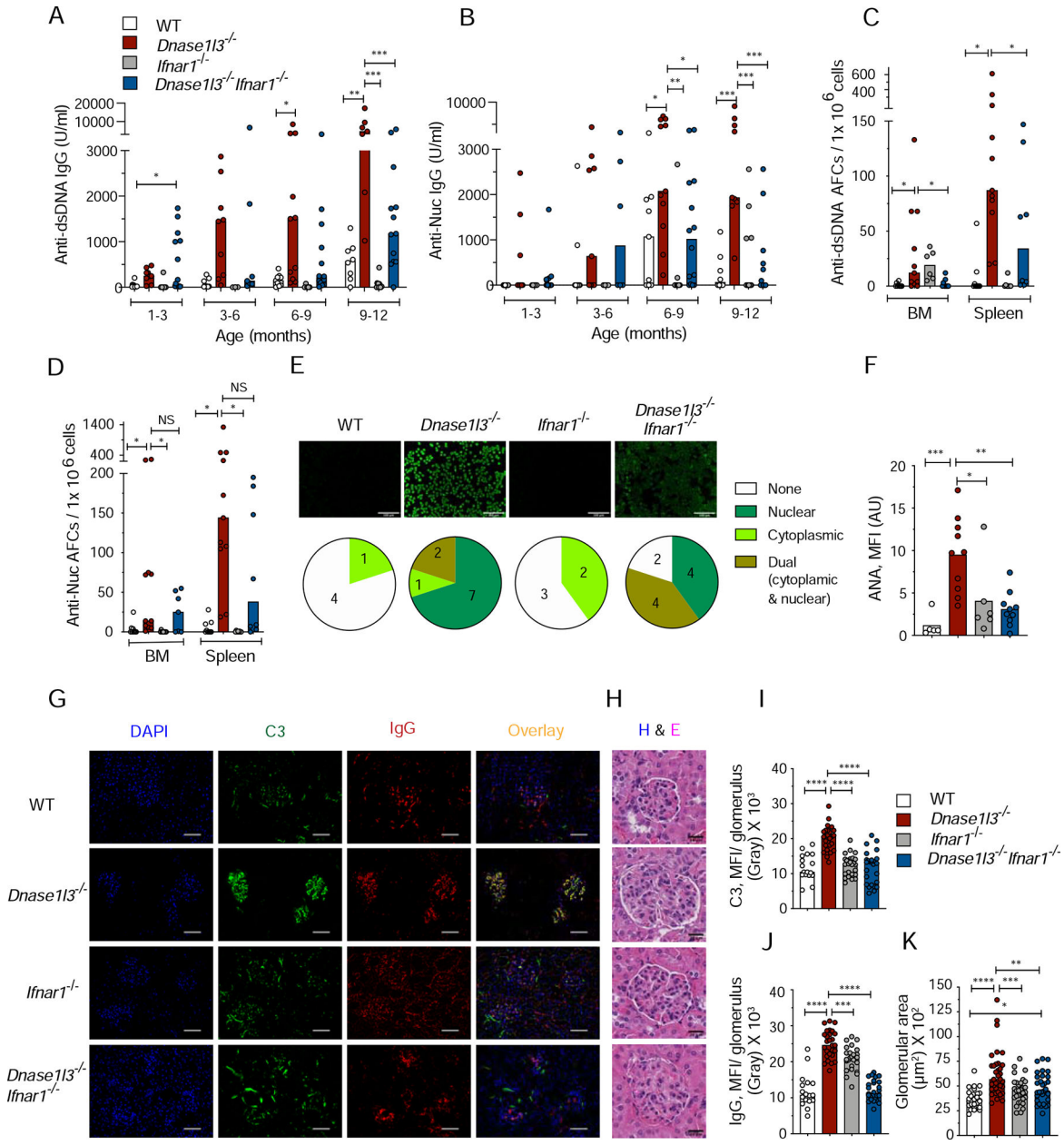

Figure 4. Autoreactivity and autoimmune manifestations in *Dnase1l3*$^{-/-}$ mice are facilitated by type I interferon signaling.

Wild-type (WT), *Dnase1l3*$^{-/-}$, *Ifnar1*$^{-/-}$ and *Dnase1l3*$^{-/-}$ *Ifnar1*$^{-/-}$ mice were examined for Abs at the indicated ages or at the 12 month endpoint.

(A and B) Serum anti-dsDNA (A) and anti-Nucleosome (B) IgG titers determined by ELISA.

(C and D) ELISpot analysis of the number of anti-dsDNA (C), and anti-nucleosome (D) antibody forming cells (AFCs) in bone marrow (BM) or spleen cells.

(E) Images of HEp-2 cells stained with sera to detect ANAs (representative of n≥ 5 per strain). Scale bars, 100 µm. Pie charts with numbers indicate distribution of ANA reactivity patterns in mice from each group.

(F) Quantitation of ANA fluorescence intensity.

(G-K) Images of kidney sections representative of ≥ 3 mice per group stained for IgG, (red) and C3 (green) and DAPI (blue). Scale bars, 40 μm, (G). Images of glomeruli from H&E-stained kidney sections, representative of ≥3 mice per group. Scale bars 20 μm (H). Quantitation of mean fluorescence intensity of C3 (I), and IgG deposits (J), and size of ≥ 20 glomeruli per kidney section (K) from 3–4 mice per strain.

In panels A-D and F, symbols represent individual mice. Panels I-K each symbol represents an individual glomerulus. All bars indicate median.

NS= not significant, * $p \leq 0.05$, ** $p \leq 0.01$, *** $p \leq 0.001$ and **** $p \leq 0.0001$.

See also Figure S4.

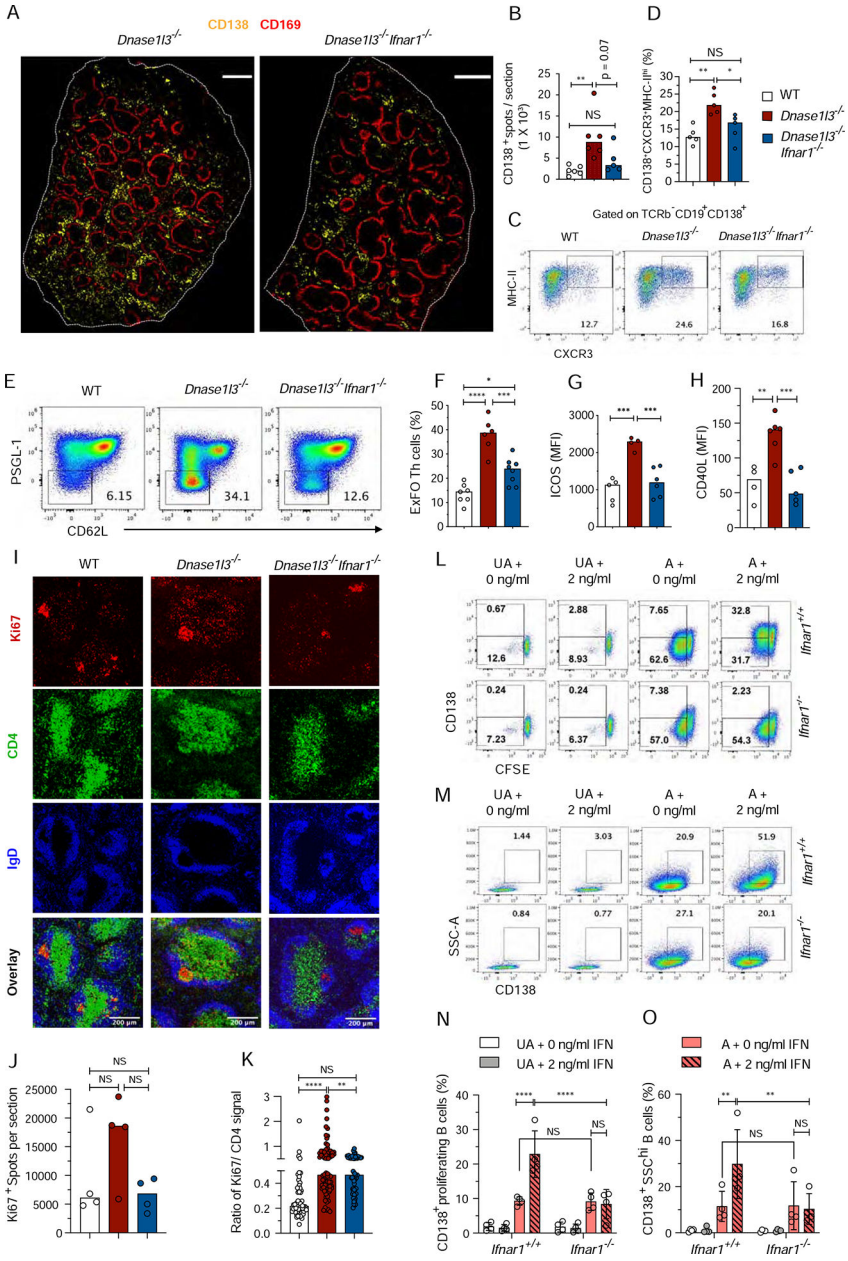

Figure 5. Type I IFN signaling promotes extrafollicular B cell proliferation and differentiation into antibody-forming cells

.

(A, B) Confocal images of half spleens representative of >4, 8–9-mo-old WT, *Dnase1l3*$^{-/-}$ and *Dnase1l3*$^{-/-}$ *Ifnar1*$^{-/-}$ mice, stained for CD169 (red) and CD138^{+} (yellow). Scale bar, 1000 μm (A); Total number of CD138^{+} spots per half spleen represented in A (B). Each symbol represents half a spleen section

(C, D) Staining profiles of gated splenic CD19^{+}CD138^{+} cells (CXCR3^{+}MHC-II^{hi} ExFO B cells highlighted) (C), and frequencies of ExFO B cells (D), in >10-mo-old WT, *Dnase1l3*$^{-/-}$ and *Dnase1l3*$^{-/-}$ *Ifnar1*$^{-/-}$ mice.

(E-H) Flow cytometric staining profiles of gated splenic $CD4^+$ T cells ($PSGL\text{-}1^{lo}CD62L^{lo}$ExFO Th cells highlighted) (E); Fraction of ExFO Th cells among splenic $CD4^+$ T cells (F), mean fluorescence intensity of ICOS (G), and CD40L (H) expressed in ExFO Th cells of 6–8-mo-old WT, *Dnase1l3*$^{-/-}$ and *Dnase1l3*$^{-/-}$*Ifnar1*$^{-/-}$ mice. In panels C-H, wherever applicable, symbols represent individual mice and bars indicate median.

(I-K) Confocal images of spleen sections representative of three >8-mo-old WT, *Dnase1l3*$^{-/-}$ and *Dnase1l3*$^{-/-}$*Ifnar1*$^{-/-}$ mice stained for $Ki67^+$ proliferating cells (red), $CD4^+$ T cells (green) and IgD^+ B cells (blue). Scale bars, 200 μm (I); Quantitation of total number of $Ki67^+$ spots per half spleen represented in Fig. S5B. Each symbol represents half a spleen section (J); Ratio of mean fluorescence intensity of Ki67 vs CD4 within a region of interest (ROI) marking $CD4^+$ T cell zones excluding GC areas, from spleen sections represented in Fig.S5B. Each symbol represents a single ROI (K).

(L-O) Flow cytometric analysis of proliferation and differentiation of B cells upon in-vitro activation with anti-IgM and anti-CD40 in the presence or absence of IFNα. Shown are representative flow plots from 4 independent experiments of purified CFSE labeled unactivated (UA) or activated (A) B cells from *Ifnar*$^{+/+}$ or *Ifnar1*$^{-/-}$ mice cultured for 72h in the absence (0 ng/ml) or presence of 2 ng/ml of IFNα. The cells in the gates indicate $CFSE^{lo}$ proliferating B cells, with (upper gate) or without (lower gate) CD138 expression (L); or $CD138^+SSC^{hi}$ B cells (M), under the indicated conditions. Fraction of $CD138^+$ proliferating (N) and $CD138^+SSC^{hi}$ blasting (O) B cells. Each symbol represents an independent experiment. Error bars show mean ± SD. Two-way ANOVA followed by Tukey's multiple-comparison test was used to compare different treatments within a genotype or 2-way ANOVA followed by Sidak's multiple comparison test was used to compare different treatments between the two genotypes. NS= not significant, * $p \leq 0.05$, ** $p \leq 0.01$, *** $p \leq 0.001$ and **** $p \leq 0.0001$.

See also Figure S5.

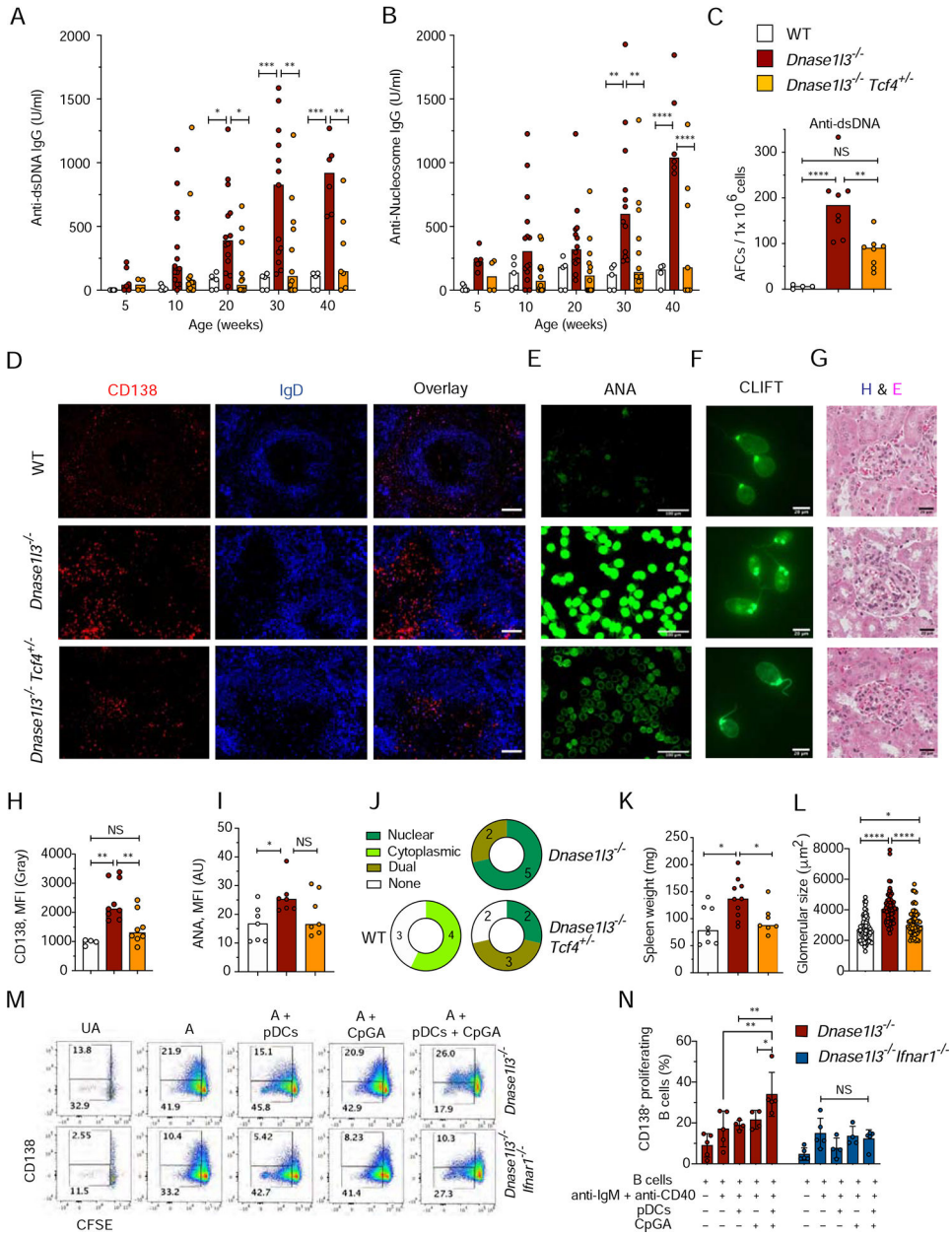

Figure 6. Functional impairment of pDCs in *Dnase1l3*$^{-/-}$ mice ameliorates autoreactivity and disease.

Wild-type (WT), *Dnase1l3*$^{-/-}$, and *Dnase1l3*$^{-/-}$ mice with monoallelic deficiency of *Tcf4* (*Dnase1l3*$^{-/-}$ *Tcf4*$^{+/-}$) were examined for Abs at the indicated ages or at the 12 month endpoint.

(A-B) Serum anti-dsDNA IgG (A) and anti-Nucleosome (B) IgG titers by ELISA.

(C) Frequency of anti-dsDNA AFCs in the spleen by ELISpot.

(D) Spleen sections stained for CD138^{+} cells (red) and follicular B cells (blue). Representative of ≥3 mice per group. Scale bars 40 μm.

(E) ANA assay images, representative of 7 mice per group. Scale bar, 100 μm.

(F) CLIFT assay for anti-dsDNA IgG (representative of 5 mice per group). Scale bar: 20 μm.

(E) Glomeruli from H&E-stained kidney sections (representative of 3 mice per group). Scale bars, 20 μm.

(H) Intensity of CD138 fluorescence in ≥ 4 images of spleen sections from the indicated mice.

(I, J) Quantitation of ANA fluorescence intensity (I), and distribution of ANA reactivity patterns (J) in 7 mice per indicated group.

(K) Spleen weights of indicated mice at the endpoint.

(L) Quantitation of the size of ≥ 20 glomeruli per kidney section from 3 mice per group. Each symbol represents an individual glomerulus; bars indicate median.

(M-N) Purified CFSE labeled B cells from *Dnase1l3*$^{-/-}$ or *Dnase1l3*$^{-/-}$ *Ifnar1*$^{-/-}$ mice were left unactivated (UA); activated with anti-IgM + anti-CD40 (A); OR activated with anti-IgM + anti-CD40 in the presence of unstimulated pDCs (A+ pDCs); in the presence of 1μM CpGA (A+ CpGA) or in the presence of pDCs stimulated with 1μM CpGA (A+ pDCs+ CpGA) for 72h after which the B cells were analyzed for proliferation and differentiation using flow cytometry. Gating strategy (M) and quantitation (N) of CFSE^{lo}CD138^{+} proliferating B cells. Error bars show mean ± SD from four independent experiments (symbols). NS= not significant, * $p \leq 0.05$, ** $p \leq 0.01$, *** $p \leq 0.001$ and **** $p \leq 0.0001$. See also Figure S6.

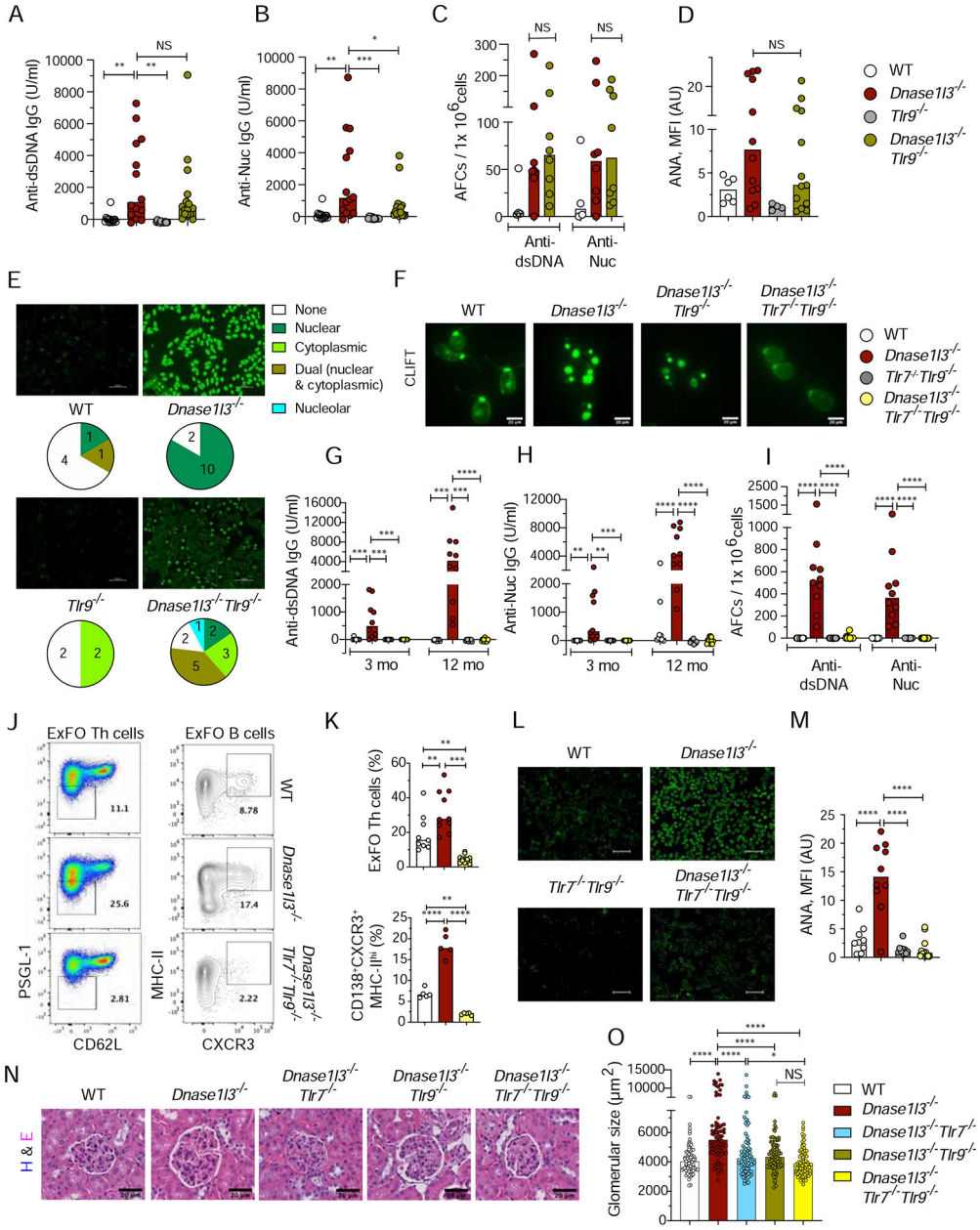

Figure 7. TLR9 and TLR7 are redundantly required for autoreactivity and autoimmunity

Wild-type (WT), *Dnase1l3*$^{-/-}$, *Tlr9*$^{-/-}$, *Tlr7*$^{-/-}$ mice or crosses thereof were examined for Abs at the indicated ages or at the 12 month endpoint.

(A-B) Serum anti-dsDNA IgG (A) and anti-Nuc (B) IgG titers by ELISA.

(C) Frequency of anti-dsDNA and anti-Nuc AFCs in the spleen by ELISpot.

(D, E) ANA assay, showing quantitation of fluorescence intensity (D), representative images and the distribution of reactivity patterns in mice from each group (E).

(F) CLIFT assay for anti-dsDNA IgG (representative of ≥4 mice per strain). Scale bar: 20 μm.

(G-H) Serum anti-dsDNA IgG (A) and anti-Nucleosome (B) IgG titers by ELISA.

(I) Frequency of anti-dsDNA and anti-nucleosome AFCs in the spleen as determined by ELISpot.

(J) Staining profiles of gated splenic $CD4^+$ T cells ($PSGL\text{-}1^{lo}CD62L^{lo}$ ExFO Th cells highlighted) and $CD19^+$ $CD138^+$ cells ($CXCR3^+$ $MHC\text{-}II^{hi}$ ExFO B cells highlighted).

(K) Frequencies of populationss highlighted in J at the endpoint.

(L-M) ANA assay, showing images representative of ≥8 mice per strain (L), and quantitation of fluorescence intensity (M). Scale bars, 100μm.

(N) Glomeruli from H&E-stained kidney sections (representative of 4 mice per group). Scale bars, 20 μm.

(O) Size of ≥ 20 glomeruli per kidney section from 4 mice per group.

Symbols represent individual mice except in panel O, where they represent individual glomeruli. All bars indicate median.

NS= not significant, * $p \leq 0.05$, ** $p \leq 0.01$, *** $p \leq 0.001$ and **** $p \leq 0.0001$.

See also Figure S7.

KEY RESOURCES TABLE

REAGENT or RESOURCE	SOURCE	IDENTIFIER
Antibodies		
V450- anti-mouse CD19 (1D3)	BD Biosciences	Cat # 560375; RRID:AB_1645269
PE/Cy7 anti-mouse CD4 (RM4–5)	eBioscience	Cat # 25-0042-82; RRID:AB_469578
APC-anti-mouse CD4 (GK1.5)	eBioscience	Cat # 17-0041-81; RRID:AB_469319
BV711-anti-mouse CD4 (RM4–5)	BioLegend	Cat # 100549; RRID:AB_11219396
PE anti-mouse CD11b (M1/70)	eBioscience	Cat # 12-0112-81; RRID:AB_465546
FITC anti-mouse CD11c (N418)	eBioscience	Cat # 11-0114-82; RRID:AB_464940
AF700 anti-mouse CD44 (IM7)	BD Pharmingen	Cat # 560567; RRID:AB_1727480
APC anti-mouse CD44 (IM7)	eBioscience	Cat # 17-0441-83; RRID:AB_469391
PeCy7 anti-mouse CD69 (H1.2F3)	eBioscience	Cat # 25-0691-81; RRID:AB_469636
PE anti mouse PD-1 (29F.IA12)	BioLegend	Cat # 135205; RRID:AB_1877232
BV605 anti-mouse ICOS (C398.4A)	BioLegend	Cat # 313537; RRID:AB_2687078
PE anti-mouse CD162 (PSGL-1) (2PH1)	BD Pharmingen	Cat # 555306; RRID:AB_395719
BV711 anti-mouse CD40L (MR1)	BD Bioscience	Cat # 740685; RRID:AB_2740371
PE anti-mouse CD138 (281–2)	BD Pharmingen	Cat # 561070; RRID:AB_2033998
PEy7 anti-mouse CD138 (281–2)	BioLegend	Cat # 142514; RRID:AB_2562198
FITC anti-mouse CD62L (MEL-14)	eBioscience	Cat # 11-0621-82; RRID:AB_465109
PerCP/Cy5.5 anti-mouse CD25 (PC61)	BioLegend	Cat # 102029; RRID:AB_893291
Pacific Blue anti-mouse B220 (RA3–6B2)	BioLegend	Cat # 103227; RRID:AB_492876
BV605 anti-mouse B220 (RA3–6B2)	BioLegend	Cat # 103243; RRID:AB_11203907
Alexa Fluor 488 anti-mouse FOXP3 (FJK-16S)	eBioscience	Cat # 53-5773-82; RRID:AB_763537
FITC Rat and mouse T and B cell activation antigen (GL-7)	BD Pharmingen	Cat # 562080; RRID:AB_10894953
APC anti-mouse IgD (11–26c.2a)	BioLegend	Cat # 405714; RRID:AB_10643423
FITC anti-mouse IgM (II/41)	eBioscience	Cat # 11-5790-81; RRID:AB_465244
PerCP/Cy5.5 anti-mouse Sca-I (D7)	eBioscience	Cat # 45-5981-82; RRID:AB_914372
PE/Cy anti-mouse Sca-I (D7)	eBioscience	Cat # 25-5981-81 ; RRID:AB_469668
AF700 anti-mouse MHC-II (M5/114.15.2)	eBioscience	Cat # 56-5321-82; RRID:AB_494009
PE/Cy7 anti-mouse Ly6G (1A8)	BioLegend	Cat # 127617; RRID:AB_1877262
APC anti-mouse Ly6C (HK1.4)	eBioscience	Cat # 17-5932-82; RRID:AB_1724153
PE anti-mouse Ki67 (16A8)	BioLegend	Cat # 652403; RRID:AB_2561524
PE anti-mouse IFNAR (AR1–5A3)	BioLegend	Cat # 127312; RRID:AB_2248800
PerCP/Cy5.5 anti-mouse CXCR4 (2B11)	eBioscience	Cat # 46-9991-80; RRID:AB_10670192
BV711 anti-mouse Siglec-H (440c)	BD Bioscience	Cat # 747671; RRID:AB_2744232
FITC goat anti-mouse C3	Immunology Consultants Laboratory Inc	Cat # GC3–90F-Z
FITC rat anti-mouse kappa (187.1)	SouthernBiotech	Cat # 1170–02; RRID:AB_2794663
PE goat anti-mouse IgG F(ab)’ Polyclonal	eBioscience	Cat # 12-4010-82; RRID:AB_11063706
Biotin anti-mouse IgG polyclonal	eBioscience	Cat # 13-4013-85; RRID:AB_466650

REAGENT or RESOURCE	SOURCE	IDENTIFIER
Biotin anti-mouse IgM (II/41)	eBioscience	Cat # 13-5790-81; RRID:AB_466674
Biotin anti-mouse IgD (11–26c (11–26)	eBioscience	Cat # 13-5993-81; RRID:AB_466859
Biotin anti-mouse CD19 (1D3)	eBioscience	Cat # 13-0193-82; RRID:AB_657656
Biotin anti-mouse CD93 (AA4.1)	eBioscience	Cat # 13-5892-81; RRID:AB_466766
Biotin anti-mouse CD5 (53–7.3)	eBioscience	Cat # 13-0051-81; RRID:AB_466338
Biotin anti-mouse Ly6G	BioLegend	Cat # 127603; RRID:AB_118610
Biotin anti-mouse Ter-119 (TER-119)	eBioscience	Cat # 13-5921-81; RRID:AB_466796
Biotin anti-mouse CD41 (MWReg30)	BioLegend	Cat # 133930; RRID:AB_2572133
Biotin anti-mouse NK1.1 (PK136)	eBioscience	Cat # 13-5941-81; RRID:AB_466803
Biotin anti-mouse TCRß (H57–597)	eBioscience	Cat # 13-5961-81; RRID:AB_466818
Biotin anti-mouse CD3e (145–2C11)	BioLegend	Cat # 100303; RRID:AB_350220
Biotin anti-mouse CD11b (M1/70)	eBioscience	Cat # 13-0112-81; RRID:AB_466358
Biotin anti-mouse CD24 (M1/69)	eBioscience	Cat # 13-0242-81; RRID:AB_466396
Biotin anti-mouse F4/80 (BM8)	eBioscience	Cat # 13-4801-81; RRID:AB_466656
Biotin anti-mouse CXCR5 (2G8)	BD Biosciences	Cat # 551960; RRID:AB_394301
Biotin anti-mouse IgG2a/2b (R2–40)	BD Biosciences	Cat # 553398; RRID:AB_394836
Biotin anti-mouse CD43 (eBioR2/60)	eBioscience	Cat # 13-0431-82; RRID:AB_466439
Alkaline phosphatase conjugated goat anti-mouse IgG	Jackson Immunoresearch	Cat # 115-055-071; RRID:AB_2338535
Mouse IgG-UNLB (Unconjugated) normal mouse serum	SouthernBiotech	Cat # 0107–01 ; RRID:AB_2732898
Goat Anti-Mouse IgG-UNLB	SouthernBiotech	Cat # 1010–01; RRID:AB_2794121
TruStain FcX anti-mouse CD16/32 (93)	BioLegend	Cat # 101319; RRID:AB_1574973
BV421 anti-mouse CD183 (CXCR3–173)	BioLegend	Cat # 126529; RRID:AB_2563100
InVivoMAb mouse IgG2a isotype control (C1.18.4)	Bio × Cell	Cat # BE0085; RRID:AB_1107771
Purified mouse-anti-CD20 (5D2)	Genentech, Inc.	NA
F(ab)'2 fragment goat anti-mouse IgM, µ chain specific	Jackson ImmunoResearch	Cat # 115-006-075
LEAF purified anti-mouse CD40	BioLegend	Cat # 102810
Chemicals, Peptides, and Recombinant Proteins		
Nucleosome antigen, calf thymus	Arotec Diagnostics	Cat # ATN02
Deoxyribonucleic acid, calf thymus	Calbiochem	Cat # 2618
Poly-L-lysine solution	Sigma Aldrich	Cat # P8920–100ML
Non-Fat Dry Milk	LabScientific	Cat # M-0841
Pierce Diethanolamine Substrate Buffer (5X)	Thermo Scientific	Cat # 34064
Phosphatase substrate	Sigma Aldrich	Cat # S0942–200TAB
ANA substrate slides	Antibodies Incorporated	Cat # 15–123
Crithidia luciliae sensitive (anti-dsDNA) indirect immunofluorescence test	Euroimmun	Cat # FA 1572-1010-1
ELISPot plates	Millipore	Cat # MSIPS4W10
Fetal Bovine Serum	Sigma Aldrich	Cat # F0926–500
VECTOR Blue alkaline phosphatase (Blue AP) substrate kit	Vector Laboratories	Cat # SK-5300
EDTA	Fisher	Cat # BP24821

REAGENT or RESOURCE	SOURCE	IDENTIFIER
Neutral Buffered Formalin (10%)	Thermo Scientific	Cat # 22-050-104 (5701)
Ethanol, Absolute	Fisher Scientific	Cat # BP2818–500
Tissue Plus O.C.T. Compound	Thermo Fisher Scientific	Cat # 23-730-571
Acetone	Fisher Scientific	Cat # A18–1
DAPI (4’,6 Diamidino 2 Phenylindole, Dilactate)	Thermo Fisher Scientific	Cat # D3571
Paraformaldehyde 4% in PBS	Thermo Fisher Scientific (Alfa Aesar)	Cat # J19943-K2
Cyclophosphamide monohydrate (CYTOPAC)	Sigma Aldrich	Cat # C7397–1G
2’-deoxy-ethyryluridine (EdU)	Carbosynth	Cat # NE08701
Recombinant mouse IFNa1 (carrier free)	BioLegend	Cat # 751804
ODN2216 (CpGA)	Invivogen	Cat # Tlrl-2216–1
Recombinant mouse IL-4 protein	R&D systems	Cat # 404-ML-010
RPMI medium 1640 with L-glutamine	Gibco	Cat # 11875–119
L-glutamine 200mM	Thermo Fisher Scientific	Cat # 25030–164
Beta-mercaptoethanol	Sigma Aldrich	Cat # 444203–250ML
Penicillin-Streptomycin 10,000U/ml	Gibco	Cat # 15140122
RBC lysis buffer	BioLegend	Cat # 420301
Live/Dead fixable aqua dead cell stain	Thermo Fisher Scientific	Cat # L34965
Bovine serum albumin	Sigma Aldrich	Cat # A9647–100G
Sucrose	Sigma Aldrich	Cat # S0389–1 KG
LPS-EK Ultrapure	Invivogen	Cat # Tlrl-peklps
Trizol LS reagent	Ambion	Cat # 10296028
Streptavidin PerCP/Cy5.5	eBioscience	Cat # 45-4317-82
Streptavidin PE/Cy7	eBioscience	Cat # 25-4317-82
Prolong Diamond antifade	Thermo Fisher Scientific	Cat # P36961
Critical Commercial Assays		
Click-iT™ EdU Alexa Fluor™ 647 Flow Cytometry Assay Kit	Thermo Scientific	Cat # C10419
RNeasy Mini Kit	Qiagen	Cat # 74104
SuperScript IV First strand synthesis system	Thermo Fisher Scientific	Cat # 18091050
FastStart high fidelity PCR system	Roche Applied Science	N/A
Lumikine mIFNa bioluminescence ELISA kit	Invivogen	Cat # lumi-mifna
Streptavidin microbeads	Miltenyi Biotec	Cat # 130-048-101
FOXP3/transcription factor staining buffer set	eBioscience	Cat # 00–5523
Deposited Data		
Experimental Models: Organisms/Strains		
Mouse: WT: C57BL/6J	The Jackson Laboratory	Stock # 000664; RRID:IMSR_JAX:000664
Mouse: WT: 129SvEvTac	Taconic Farms	Model # 129SVE-F or 129SVE-M; RRID:IMSR_TAC:129sve
Mouse: *Dnase1l3*$^{-/-}$ [B6NCrl.Cg-*Dnase1l3*$^{tm1c(KOMP)Wtsi/TwinMmucd}$]	Taconic animal repository	Model TF2732; RRID:MMRRC_065348-UCD

REAGENT or RESOURCE	SOURCE	IDENTIFIER
Mouse: *Cd40lg*$^{-/-}$ [B6.129S2-*Cd40lg*^{tm1Imx}/J]	The Jackson Laboratory	Stock # 002770; RRID:IMSR JAX:002770
Mouse: *Tlr7*$^{-/-}$ [B6.129S1-*Tlr7*^{tm1Flv}/J]	The Jackson Laboratory	Stock # 008380; RRID:IMSR JAX:008380
Mouse: *Ifnar1*$^{-/-}$ [B6.129S2-*Ifnar1*^{tm1Agt}/Mmjax]	The Jackson Laboratory	Stock # 032045-JAX; RRID:MMRRC 032045-JAX
Mouse: *Tcf4*$^{+/-}$ [B6;129- *Tcf4*^{tm1Zhu}/J]	The Jackson Laboratory	Stock No: 013598 RRID:MGI :3040597
Mouse: C57BL/6J-*Tlr9*^{M7Btir}/Mmjax	The Jackson Laboratory	MMRRC Stock No. 34329-JAX/ CpG11 ; RRID:MMRRC 034329-JAX
Oligonucleotides		
VH Forward Primers Primer (5’ -> 3’)		
mVH-Fwd1 GAKGTRMAGCTTCAGGAGTC	Sigma Aldrich	N/A
mVH-Fwd2 GAGGTBCAGCTBCAGCAGTC	Sigma Aldrich	N/A
mVH-Fwd3 CAGGT GCAGCT GAAGSASTC	Sigma Aldrich	N/A
mVH-Fwd4 GAGGTCCARCTGCAACARTC	Sigma Aldrich	N/A
mVH-Fwd5 CAGGTYCAGCTBCAGCARTC	Sigma Aldrich	N/A
mVH-Fwd6 CAGGTYCARCTGCAGCAGTC	Sigma Aldrich	N/A
mVH-Fwd7 CAGGT CCACGT GAAGCAGT C	Sigma Aldrich	N/A
mVH-Fwd8 GAGGT GAASST GGTGGAATC	Sigma Aldrich	N/A
mVH-Fwd9 GAVGTGAWGYTG GTGGAGTC	Sigma Aldrich	N/A
mVH-Fwd10 GAGGT GCAGSKGGT GGAGT C	Sigma Aldrich	N/A
mVH-Fwd11 GAKGTGCAMCTGGTGGAGTC	Sigma Aldrich	N/A
mVH-Fwd12 GAG GT GAAG CTGATGGARTC	Sigma Aldrich	N/A
mVH-Fwd13 GAGGT GCARCTT GTT GAGT C	Sigma Aldrich	N/A
mVH-Fwd14 GARGTRAAGCTTCTCGAGTC	Sigma Aldrich	N/A
mVH-Fwd15 GAAGT GAARSTT GAGGAGT C	Sigma Aldrich	N/A
mVH-Fwd16 CAGGTTACTCTRAAAGWGTSTG	Sigma Aldrich	N/A
mVH-Fwd17 CAGGTCCAACTVCA GCARCC	Sigma Aldrich	N/A
mVH-Fwd18 GAT GT GAACTTGGAAGT GT C	Sigma Aldrich	N/A
mVH-Fwd19 GAG GT GAAG GT CAT CGAGTC	Sigma Aldrich	N/A
VH Reverse Primers Primer (5’ -> 3’)		

REAGENT or RESOURCE	SOURCE	IDENTIFIER
mVH-Rev-IgG CCARKGGATAGACHGATGGGG	Sigma Aldrich	N/A
mVH-Rev-IgA TGGTGGGATTTCTCGCAGAC	Sigma Aldrich	N/A
mVH-Rev-IgM GCAGGAGACGAGGGGGAAGA	Sigma Aldrich	N/A
Software and Algorithms		
ImageJ	https://imaqei.nih.qov/ij/	RRID:SCR_001935
CTL Immunospot analyzer	http://www.immunosDot.com/ImmunoSpot-analyzers-software	RRID:SCR_011082
Adobe Photoshop CC2018	https://www.adobe.com/products/photoshop.html	RRID: SCR_014199
Adobe Illustrator CC2018	https://www.adobe.com/products/illustrator.html	RRID: SCR_010279
FLowjo v10	Treestar Inc	RRID: SCR_008520
GraphPad Prism 7	Graphpad Inc	RRID: SCR_002798
Imaris	http://www.bitplane.com/imaris/imaris	RRID: SCR 007370
Keyence BZ Analyzer software	https://www.keyence.co.iD/Droducts/microscoDe/fluorescence-microscoDe/bz-8100/models/bz-h1a/	RRID:SCR_017205
Slidepath Gateway digital pathology	Leica Microsystems	RRID:SCR_005597